Hydrodynamics of Unitary Fermi Gases

by

Ryan E. Young

B.A., University of Colorado at Boulder, 2011

A thesis submitted to the

Faculty of the Graduate School of the

University of Colorado in partial fulfillment

of the requirements for the degree of

Master of Applied Mathematics

Department of Applied Mathematics

2013

This thesis entitled:
Hydrodynamics of Unitary Fermi Gases
written by Ryan E. Young
has been approved for the Department of Applied Mathematics

Paul Romatschke

Anna Maria Rey

Anne Dougherty

Date

The final copy of this thesis has been examined by the signatories, and we find that both the content and the form meet acceptable presentation standards of scholarly work in the above mentioned discipline.

Young, Ryan E. (MA., Applied Mathematics)

Hydrodynamics of Unitary Fermi Gases

Thesis directed by Prof. Paul Romatschke

Unitary fermi gases have been widely studied as they provide a tabletop archetype for research on strongly coupled many body systems and perfect fluids. Research into unitary fermi gases can provide insight into may other strongly interacting systems including high temperature superconductor, quark-gluon plasmas, and neutron stars. Within the unitary regime, the equilibrium transport coefficients and thermodynamic properties are universal functions of density and temperature. Thus, unitary fermi gases provide a archetype to study nonperturbative many-body physics, which is of fundamental significance and crosses several fields.

This thesis reports on two topics regarding unitary fermi gases. A recent string theory conjecture gives a lower bound for the dimensionless ratio of shear viscosity of entropy, $\eta/s \geq 4\pi\hbar/k_b$. Unitary fermi gases are a candidate for prefect fluids, yet η/s is well above the string theory bound. Using a stochastic formulation of hydrodynamics, we calculate a lower bound for this ratio accounting for the momentum dissipation from fluctuations. This lower bound is in good agreement with both theoretical and experimental results.

The second question addressed is the simulation of elliptic flow. Elliptic flow, first observed in 2002, is a characteristic of strongly coupled systems and has been studied in both quark-gluon plasmas and unitary fermi gases. As such, simulations of these systems are of interest. We test a variety of lattice Boltzmann models and compare the simulation results to the theoretical and experimental findings.

Contents

Chapter

Figures

Figure

Chapter 1

Introduction

1.1 Unitary Fermi Gases

1.1.1 Introduction

The realization of Bose-Einstein condensation (BEC) in dilute atomic vapors ushered in an era of exploring unique and fascinating physics [3] [9] [16] . In these system, weakly interacting bosonic atoms are confined via laser trapping systems and cooled to ultra low temperature regimes where quantum behavior dominates. This offers a tunable tabletop archetype to study many body physics.

The study of BEC is an actively thriving field, but a new regime of ultra cold quantum degenerate Fermi gasses is now being realized. Quantum degeneracy occurs when, as the gas is cooled, the particles' wave packets, whose characteristic size is given by the thermal de Broglie wavelength $\lambda_T = h/\sqrt{2\pi m k_b T}$, grow and begin to overlap. This happens when the interatomic distance L, is on the order of the de Broglie wavelength $\lambda_T \sim L$. For bosons, particles that can share quantum states, this degeneracy is not a problem as they crowd into the same quantum state and form a condensate. The Pauli exclusion principle dictates that fermions can not share the same quantum state. This is expected to suppress three-body recombination creating a unique system of stable strongly interacting degenerate fermi gas. In contrast, three body collisions make strongly interacting bosonic gasses unstable.

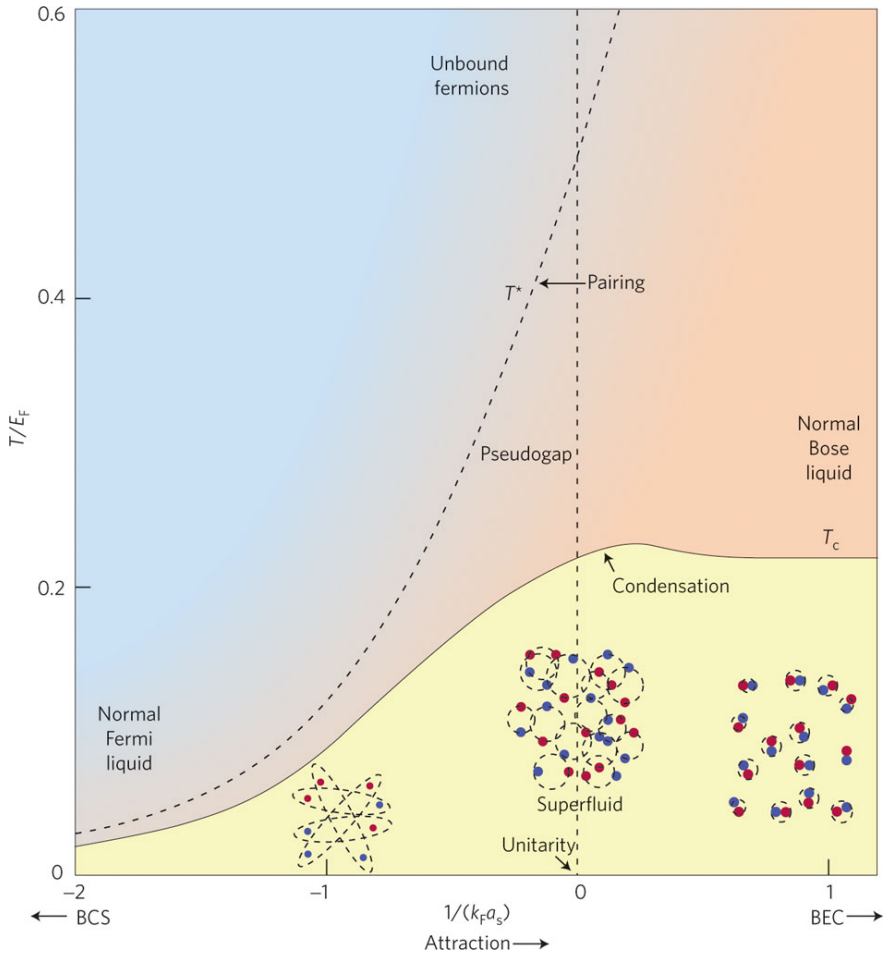

Figure 1.1: A schematic phase diagram of an ultracold fermi gas showing the evolution from the ground state of the BCS limit with large, spatially overlapping Cooper pairs to the BEC limit with tightly bound molecules. The ground state at unitarity, $1/(ka_s) = 0$, has strongly interacting pairs whose size is on the order of $1/k$. As a function of increasing attraction, the pair-formation crossover scale T^* diverges away from T_c below which a condensate exists. Most fermi superfluids and superconductors are close to the BCS limit where these two temperatures coincide. Reproduced from [1].

A unique state of a cold fermi gas is the unitary limit, where the equation of state is similar to that of an ideal gas. That is, the pressure is given by $p = 2/3\mathcal{E}$, where $\mathcal{E}$ is the energy density. Let us now delve into the physics of this unique state. Let us consider a gas of two species of non-relativistic fermions, labelled species a and b, respectively, that interact with a short ranged

attractive potential. For simplicity, assume the masses are equal $m_a = m_b = m$, and the total density is $n_+ = n_a + n_b$. Everything shall be expressed in terms of the fermi energy $\epsilon_F = \hbar^2 k_F^2/2m$, and the wave vector k_F.

At low density, the dominant interaction is the s-wave, or shear wave interaction. It is well described by the effective range expansion

$$k \cot(\delta_k) = \frac{-1}{a_s} + \frac{r_e k^2}{2} + O(k^4) \tag{1.1}$$

where δ_k is the phase shift at wave-vector k, and r_e is the effective range. The above equation serves as one method of defining the s-wave scattering length a_s. The unitary limit is the separation of length scales.

$$r_e \ll k_f^{-1} \ll a_s \tag{1.2}$$

This is the regime where the density is so low that the inter-particle separation is much larger than the interaction range $k_f r_e \ll 1$ and the scattering length diverges $a_s \to \infty$. The properties of the potential are given by higher order terms in the range expansion, Eq(1.1), that become irrelevant. In the unitary limit, everything is characterized by the lack of an intrinsic length scale and therefore is universal.

The physics of homogeneous matter described by a single dimensionless parameter, $(k_f a_s)^{-1}$, is described by the theories of Bardeen-Cooper-Schrieffer (BCS)/Bose-Einstein Condensate (BEC) crossover. In the unitary limit the scattering length is much larger than the inter-particle spacing, $1 \ll |k_F a_s|$. At this point, the other length scales fail to be important and a theory is needed whose one dimensionfull scale is set by the density $n_+ = k_F^3/3\pi^2$.

A result of the universality is that the thermodynamic properties are simply defined by an ideal gas like expression.

$$\mathcal{E}(n_+) = \xi \mathcal{E}_{FG}(n_+) \tag{1.3}$$

where $\xi \approx .37$ is the the dimensionless Bertsch parameter and $\mathcal{E}_{FG}$ is the energy density of a free Fermi gas. Despite the simplistic thermodynamics, analytic and experimental progress has been hard won. The highly correlated nature of the system and lack of a perturbative expansion parameter has made accurate measurement or calculation of ξ challenging. See Fig(13) of [19] for a historical set of ξ values.

1.1.2 Motivation for Studying Unitary Fermi Gases

Unitary fermi gases provide an experimentally realizable system that can be connected to a number of strongly correlated systems in a wide number of fields. Many of these systems are difficult to access experimentally or to detect. Two systems of current interest that can be connect to unitary fermi gases are high temperature superconductors and quark-gluon plasmas.

The standard model is the currently accepted model describing high energy physics. There are 12 flavors of elementary Fermions, six of which are quarks. As Fermions, quarks are spin 1/2 particles and are bound to other quarks via gluon exchange to form composite particles such as protons and neutrons. At extremely high temperatures and densities quark gluon plasmas consisting of asymptotically free quarks and gluons can be formed. These high temperature and density conditions are believed to exist microseconds after the Big Bang [15].

The Relativistic Heavy Ion Collider (RHIC) at Brookhaven National Laboratory has recently produced quark gluon plasmas. This is accomplished when two gold ions are accelerated to 100 GeV per nucleon and collided. In these collisions, temperatures of $2 \times 10^{12}\ K$ and energy densities of 1 GeV/fm^3 are reached [15]. In this regime, the plasma undergoes an elliptic flow that is very similar to the flow observed in unitary Fermi gases despite 19 and 25 orders of magnitude difference in temperature and density, respectively. Moreover, the dimensionless ratio of shear viscosity to entropy of these two systems is very similar. As well, the quark gluon plasma exist for roughly 4 fm/c making it extremely difficult to study experimentally. As a result of these experimental difficulties, the unitary Fermi gas provides a more easily accessible and manipulatable system that can aid in the understanding of quark gluon plasmas.

Another strongly interacting system of interest are high temperature superconductors. A superconductor transmits electric current with almost perfect efficiency. In contrast, in ordinary metals, electric currents encounter resistance due to the frequent collisions between electrons, resulting in dissipative heating. Generally, the resistance of a metal is dependent on the temperature. For some metals, when the temperature is lowered past a critical point T_c, the resistance disappears and a superconductor is made. Raising the critical temperature is an important goal as, it would allow superconductors to be used practical electronic devises.

Fermi gases have the potential to form superfluids when sufficiently cooled. Superfluids are the gas analogue to the superconductors present in solid state physics. In contrast to bosonic superfluids, where all atoms occupy their ground state, the Pauli exclusion principle prevents clustering at the lower energy levels in fermionic fluids. BCS theory predicts that weakly interacting Fermions can form Cooper pair on top of a filled Fermi sea due to the presences of many-body effects. The critical temperature and the pair binding energy, are predicted by BCS theory to scale like $\exp[-1/(k_F|a_s|)]$. Therefore, to experimentally access the superfluid transition experimentally, the interatomic interactions must be enhanced. With strong atomic interaction, unitary Fermi gas may achieve fermionic superfluidity with a very high critical temperature.

1.2 Quantum Viscosity

1.2.1 Defining Viscosity

Viscosity is a familiar concept from our daily experience. Intuitively, viscosity is the measure of the "stickiness" of a flow, relating to how easily it flows. More precisely, viscosity is the measure of the reaction of the fluid when stress is applied. The shear viscosity is the resistance to shear stress, while the bulk viscosity is related to the changing of fluid volume. Therefore, in the incompressible limit the bulk viscosity vanishes.

In this work, we will solely be concerned with shear viscosity, as unitary fermi gasses have essentially zero bulk viscosity [50][21]. The shear viscosity can be defined as the frictional force F_x

per unit area A created by a flow with velocity gradient $\nabla_y v_x$.

$$\frac{F_x}{A} = \eta \nabla_y v_x \tag{1.4}$$

where η is the shear viscosity coefficient, commonly referred to simply as the shear viscosity. The standard unit for η is a Poise, 1 Poise= $1\mathrm{g} \cdot \mathrm{cm}^{-1} \cdot \mathrm{s}^{-1}$

Maxwell was the first to study viscosity and transport. He concluded that the shear viscosity for a dilute gas is the momentum transport of single particles. He also showed that for an ideal gas the viscosity is only dependent on temperature [10]. Consider the estimate for viscosity [47]

$$\eta = \frac{1}{3} n p l_{mfp} \tag{1.5}$$

where $n,\ p$, and l_{mfp} are the density, average thermal momentum, and mean free path, respectively. The mean free path can be expressed as $l_{mpf} = 1/(n\sigma)$, where σ is the appropriate scattering cross section. For unitary fermi gasses, this is the s-wave cross section. This gives us a viscosity not dependent on density.

$$\eta \sim \frac{p}{\sigma} \tag{1.6}$$

As mentioned previously, the unitary fermi gas at low temperatures is characterized by divergent s-wave scattering and a zero range interaction potential. In this regime, there are two length scales, the inter-particle spacing L, and the thermal wavelength λ_T. The local thermodynamic properties and transport coefficients are universal functions of density and temperature [26]. The natural momentum of a Fermi gas is on the order of $\hbar/l$ and the natural area is l^2, where l is the natural length scale. At very low temperatures, well below the temperature where degeneracy becomes relevant, the Fermi momentum set scales as $l \simeq L$. Therefore, at low temperatures the viscosity behaves as $\eta \propto \hbar/L^3 \propto \hbar n$. At temperature above where degeneracy is important, one finds $l \simeq \lambda_T \propto \hbar T^{-1/2}$, leading to a shear viscosity of $\eta \propto T^{3/2}/\hbar^2$. This scaling of $T^{3/2}$ is expected as it is well established that the viscosity for classical fluids is solely dependent on temperature.

The term quantum viscosity is used as both of the above shear viscosity scalings contain $\hbar$.

For a unitary Fermi gas with an equal number of two spin states, the viscosity can be found via the Boltzmann equation that in the high temperature limit [11]

$$\eta = \frac{45 m^{3/2} k_B^{3/2}}{32 \hbar^2 \sqrt{\pi}} T^{3/2} \tag{1.7}$$

where k_B is Boltzmann's constant and m is the atomic mass, confirming the simple scaling calculations. A more intuitively pleasing result can be written using the dimensionless ratio

$$\frac{\eta}{\hbar n} = 2.77 \left(\frac{T}{T_F} \right)^{3/2} \qquad T_F(n) = \frac{\hbar^2 (3\pi n)^{2/3}}{2 m k_B} \tag{1.8}$$

where T_F is the Fermi temperature. These scaling results will be used in both the analytic work and simulation presented later.

1.2.2 String Theory Conjecture

Recently, a universal lower bound on the ratio η/s was found by three sting theorist, Kovtun, Son, and Starinets [29].

$$\frac{\eta}{s} \geq \frac{1}{4\pi} \frac{\hbar}{k_B} \tag{1.9}$$

This bound is valid for a large general class of interacting quantum fluids, including unitary Fermi gases and quark-gluon plasmas. Fluids that saturate the bound are defined to be perfect fluids [29]. Fluids with a η/s ratio approaching this bound are nearly perfect fluids. As mentioned earlier, both unitary Fermi gas and quark-gluon plasma are good candidates for nearly perfect fluids. They also share a similar η/s despite drastic differences in temperature and density.

The η/s ratio's scaling can be understood using simple dimensional analysis. Far below the Fermi temperature, where degeneracy dominates, $\eta \propto \hbar n$ as previously noted. The entropy for a normal fluid, not a superfluid, scales as $s \simeq n k_B$, yielding $\eta/s \simeq \hbar/k_b$. This scaling can also be approached by considering the famous Heisenberg uncertainty principle which requires $p l_{mfp} \geq \hbar$.

Combining this with our previously known scaling of $\eta \propto npl_{mfp}$, we have $\eta \geq n\hbar$. This is not a useful universal quantity as in high energy physics the number of particles is not generally conserved. However, this does lead to $\eta/s \geq \hbar/k_B$, once again.

For a quark-gluon plasma and a unitary Fermi gas $\eta/s \approx 0.2,\ 0.4\ \hbar/k_b$ respectively [44]. For both systems, the string theory bound is not realized, yet these are the lowest ratios ever observed. One possible mechanism for this discrepancy is that the string theory bound does not consider fluctuation within the fluid and the effect fluctuations have on transport coefficients, such as the viscosity. In the next chapter, this mechanism is considered and a lower bound is calculated from a stochastic formulation of hydrodynamics for a unitary Fermi gas.

Chapter 2

Fluctuating Hydrodynamics

2.1 Motivation

Hydrodynamics allows for long lived shear and sound waves. Fluctuations can populate these modes and the interactions of these waves can dissipate momentum. This contributes to the shear viscosity and other transport coefficients. To see this intuitively consider a shear wave as illustrated in Fig(2.1), where a shear wave propagates from right to left. Hydrodynamics dictates that wave will decay in time as the $\hat{x}$-momentum diffuses in the $\hat{y}$ direction into regions where the fluid is stationary. This diffusion is controlled by the shear viscosity, which is by definition the diffusion coefficient for the for momentum orthogonal to the diffusion. Fluctuations can create such waves, dissipating momentum.

Our study builds upon results found in the context of relativistic fluids, specifically [31], which was recently applied to the case of the Fermi gas at unitarity by Chafin and Schäfer in [14]. In [14] it was found that the dimensionless combination of shear viscosity over density $\eta/n \geq 0.32$ for the unitary Fermi gas at the superfluid-normal phase transition temperature $T = T_c$. Thus, there is a tension between this result and the result for η/n found in the quantum Monte Carlo simulations by Wlazlowski et al. in [53], who found $\eta/n \lesssim 0.2$. This provides the motivation for us to re-derive and generalize the result by Chafin and Schäfer.

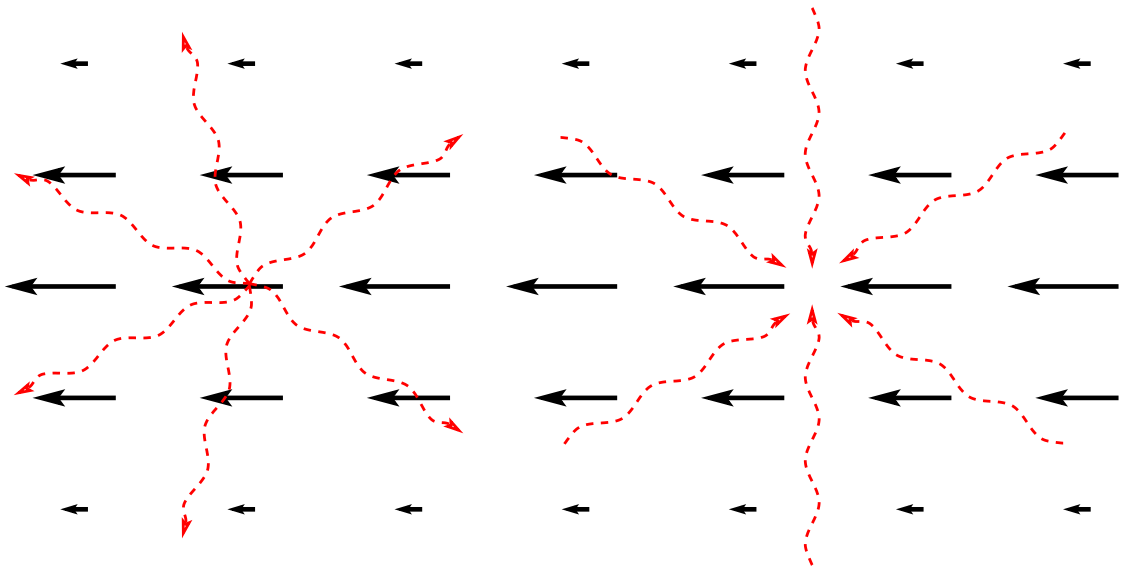

Figure 2.1: A shear wave; fluid moves to the right to left with higher velocity in the middle of the waves and low velocity at the edges. Viscosity determines the loss (by diffusion) of the forward motion of this fluid. Sound waves (dotted, in red) leaving the left-moving fluid carry, on average, net left-moving momentum, which is not compensated by sound waves arriving in the left-moving fluid. Hence sound waves contribute to viscosity. Reproduced with permission from [31].

This work is organized as follows. First, an overview of the difference between classical and fluctuating (stochastic) hydrodynamics is given. Then in section 2.3, the velocity-velocity correlator, an essential building block, is found. With the building blocks known, in section 2.4 the contribution from fluctuations to shear viscosity is calculated. In the following sections a lower bound on the viscosity is derived. This bound is dependent on the thermodynamics variables of the fermi gas. Therefore, the equation of state is found so that the thermodynamics variables can be evaluated.

2.2 Classical versus Fluctuating Hydrodynamics

This section provides, a brief overview of the difference between "classical" hydrodynamics (bare quantizes) and the physical quantizes of fluctuating hydrodynamics.

Classical hydrodynamics is the low frequency/low wavenumber effective theory of energy

momentum conservation. It can be derived from first principles by first identifying the relevant degrees of freedom (fluid velocity, particle density) and the central object (the energy momentum tensor). One then proceeds to write down all possible terms in the energy momentum tensor allowed by symmetry and ordered by the number of gradients involved. The most compact way of achieving this is using Poincaré symmetry and relativistic 4-vector notation (see [41] for a review), but all the building blocks are present in classic fluid dynamics textbooks, such as [33]. In the non-relativistic context, to zeroth order in the gradient expansion, the energy density, T_{00}, is given by the fluid mass density, $T_{00} = n$, the momentum density, T_{0i}, is given by mass density times fluid velocity, $T_{0i} = nv_i$, and the stress tensor is given by $T_{ij} = nnv_iv_j + P\delta_{ij}$ with P the fluid pressure. Energy and momentum conservation then read

$$\begin{aligned} \partial_t T_{00} + \partial_j T_{0j} &= \partial_t n + \partial_j \left(nv_j\right) = 0 \\ \partial_t T_{0i} + \partial_j T_{ij} &= \partial_t \left(nv_i\right) + \partial_j \left(nv_iv_j + P\delta_{ij}\right) = 0 \,, \end{aligned} \tag{2.1}$$

which, upon some rearrangement, can be seen to represent the equation of continuity and Euler's equation, respectively. Inclusion of derivative terms up to first order in gradients in the energy-momentum tensor leads to

$$T_{ij} = nv_iv_j + P\delta_{ij} - \eta_{\rm cl}\left(\partial_i v_j + \partial_j v_i - \frac{2}{3}\delta_{ij}\partial_k v_k\right) - \zeta_{\rm cl}\delta_{ij}\partial_k v_k \,,$$

where $\eta_{\rm cl}$ and $\zeta_{\rm cl}$ are the classical shear and bulk viscosity coefficients, respectively. It is straightforward to verify that the corresponding conservation equations are the Navier-Stokes equations. Higher-order gradient term corrections can be calculated, making the approach systematic, but these will be of no relevance to the present work and hence will not be discussed here.

It is well known that this classical hydrodynamic description, though very successful in its own right, does not do justice to the dynamics of real fluids because it does not do full justice to the fluctuation-dissipation theorem (see [30] for a recent review). This is a result of the treatment of fluids as a continuum field, instead of a collection of particles. The statistical mechanics picture is missing, in which individual particle properties are probabilistic and bulk properties are defined

as averages over all particles. However, it is well known how to alleviate this shortcoming, namely by the introduction of a stochastic noise term in the energy-momentum tensor:

$$T_{ij} \to T_{ij} = T^{\rm cl}_{ij} + \Xi_{ij}$$

where here and in the following the notation "cl" will denote classical quantities. The noise term must be chosen to accurately reproduce the equation of motion of classical hydrodynamics and model physical noise. Following the relativistic work, the noise is coupled through the projector onto symmetric traceless tensors

$$S_{\mu\nu\alpha\beta} = \frac{1}{2}\left[\Delta_{\mu\alpha}\Delta_{\nu\beta} + \Delta_{\nu\alpha}\Delta_{\mu\beta} - \frac{2}{d}\Delta_{\mu\nu}\Delta_{\alpha\beta}\right]$$

where $\Delta_{\mu\nu} = g_{\mu\nu} + u_\mu u_\nu$ and $g = \mathrm{diag}[-1,+1,+1,+1]$ is the metric tensor of a flat spacetime. The projector satisfies $S_{\mu\nu\alpha\beta}S^{\alpha\beta n\sigma} = S^{n\sigma}_{\mu\nu}$, $u^{\mu\nu}S_{\mu\nu\alpha\beta} = 0$, along with the symmetry properties $S_{\mu\nu\alpha\beta} = S_{\nu\mu\alpha\beta}$, $S_{\mu\nu\alpha\beta} = S_{\alpha\beta\mu\nu}$, and the traceless condition $g^{\mu\nu}S_{\mu\nu\alpha\beta} = 0$. The noise term is then defined as $\Xi_{\mu\nu} = \xi_{\alpha\beta}S^{\alpha\beta\mu\nu}$, where the noise $\xi_{\alpha\beta}$ has short distance gaussian correlations. In the non-relativistic limit this gives

$$\begin{aligned} \Xi^{jk} &= \frac{1}{2}(\xi^{jk} + \xi^{kj} - \frac{2}{3}\delta_{jk}\xi^{ll}) \\ \langle \xi^{ik}\xi^{nm}\rangle &= \eta T(\delta_{il}\delta_{km} + \delta_{kl}\delta_{im})\delta(x-x') \end{aligned} \tag{2.2}$$

This formulation of "fluctuating" hydrodynamics contains equations of motion of classical hydrodynamics as the average of the equations of motion over the noise, e.g.

$$\langle \partial_t T_{0i} + \partial_j T_{ij}\rangle = \partial_t T^{\rm cl}_{oi} + \partial_j T^{\rm cl}_{ij}\,, \tag{2.3}$$

because of the nature of the noise correlator. However, the two formulations, classical and fluctuating, will differ when calculating correlation functions, such as the retarded correlator of the energy-momentum tensor component T^{xy}, namely

$$G^R_{xyxy}(x-y) = \langle T_{xy}(x)T_{xy}(y)\rangle_R\,.$$

This correlator is of special interest because its Fourier transform can be related to the value of transport coefficients. For simplicity, let us restrict our treatment to the special case of a conformal system with a vanishing bulk viscosity coefficient, an excellent model for unitary fermi gasses. Then, in classical hydrodynamics, the Fourier transform of the above mentioned correlator becomes ([14], cf. [6])

$$G^{R,\mathrm{cl}}_{xyxy}(\omega,\mathbf{k}) = P - i\eta_{\mathrm{cl}}\omega + \eta\tau^{\mathrm{cl}}_R\omega^2 - \frac{\kappa^{\mathrm{cl}}}{2}\mathbf{k}^2 + \mathcal{O}(\omega^3,\mathbf{k}^3)\,, \tag{2.4}$$

with η_{cl} the classical shear viscosity coefficient as before. Here τ^{cl}_R (the relaxation time) and κ^{cl} are two transport coefficients that arise when considering hydrodynamics at second order in fluctuations (one order higher than Navier-Stokes). They will turn out to be irrelevant for the following discussion but have been included here for completeness.

As mentioned above, the stochastic formulation of hydrodynamics contains this result as a special case (with the exception of the frequency and momentum independent "contact" term P in $G^{R,\mathrm{cl}}_{xyxy}$). This is most easily seen by first realizing that at zero momentum, G^R_{xyxy} is related to another energy-momentum tensor correlator via a hydrodynamic analogue of the Ward-Takahashi identity[1]

$$\begin{aligned} G^R_{xyxy}(\omega,0) = \lim_{\mathbf{k}\to 0}\frac{\omega^2}{\mathbf{k}^2}\langle T_{0y}T_{0y}\rangle_R \;= \\ n^2\int\frac{d\omega'}{2\pi}\int\frac{d^3\mathbf{p}}{(2\pi)^3}\times \\ \Big(\Delta^{xx}_S(\omega',\mathbf{p})\Delta^{yy}_R(\omega-\omega',-\mathbf{p}) + \Delta^{xy}_S(\omega',\mathbf{p})\Delta^{yx}_R(\omega-\omega',-\mathbf{p}) + \\ \Delta^{xx}_S(\omega',\mathbf{p})\Delta^{yy}_R(\omega-\omega',-\mathbf{p}) + \Delta^{xy}_S(\omega',\mathbf{p})\Delta^{yx}_R(\omega-\omega',-\mathbf{p})\Big) \end{aligned} \tag{2.5}$$

where $\Delta^{xy}_{R,S} = \langle v_x v_y\rangle_{R,S}$, the retarded or symmetric velocity-velocity correlator. If we take $\mathbf{k} = (k,0,0)$, and $T_{0y} = nv_t$, a short calculation given in section 2.3 leads to the finding that to lowest order in fluctuations

$$\langle T_{0y}T_{0y}\rangle^{(0)}_R = n_o^2\langle v^t_y v^t_y\rangle_R = \frac{-\eta_{\mathrm{cl}}k^2}{-i\omega+\gamma k^2}$$

[1] This can be shown easily by considering correlators built out of $\partial_t T_{i0} = -\partial_j T_{ij}$.

which in turn leads to

$$G^{R,(0)}_{xyxy}(\omega,0) = -i\omega\eta_{\rm cl}\,. \tag{2.6}$$

Note that this result matches the classical hydrodynamic result Eq. (2.4) up to terms of first order in frequency. This is because it was derived using the hydrodynamic formulation including only first order gradients in the energy-momentum tensor (commonly known as Navier-Stokes equations). If higher order versions of hydrodynamics are employed, the terms involving τ_R and κ in Eq. (2.4) should also be described correctly.

Moreover, note that this result was derived keeping only the lowest order contribution in fluctuations. Clearly, correction to this result involving higher order contributions from fluctuations will also contribute to the full result. Hence

$$G^{R}_{xyxy}(\omega,0) = G^{R,(0)}_{xyxy}(\omega,0) + G^{R,(1)}_{xyxy}(\omega,0) + G^{R,(2)}_{xyxy}(\omega,0) + \dots\,,$$

where, as above, $G^{R,(0)} = G^{R,\rm cl}$. Therefore, correlation functions in fluctuating hydrodynamics will generaly differ from those calculated in classical hydrodynamics. As seen in Eq(2.5), the correlator G^R can be expressed as the integral of velocity-velocity correlators. Let us now discuss how to find such correlators.

2.3 Finding the Velocity-Velocity Correlator

To find the velocity-velocity we begin with the first order, in gradients, fluctuating hydrodynamic equations (Navier-Stokes and continuity), as higher orders are not necessary for this work.

$$\frac{\partial}{\partial t}(nv_k) + \frac{\partial T_{ik}}{\partial x_k} = 0\,, \quad \frac{\partial}{\partial t}n + \frac{\partial}{\partial x_k}(nv_k) = 0\,, \tag{2.7}$$

The noise term, Ξ_{ij}, has added to the stress tensor, $T_{ik} = T^{\rm cl}_{ik} + \Xi_{ij}$ to account for short distance fluctuations. Here we take Ξ_{ij} to be given by short distance Gaussian noise:

$$\langle \Xi_{ik}, \Xi_{nm}\rangle \;\; = \;\; \eta_{\rm cl} T\left(\delta_{in}\delta_{km} + \delta_{im}\delta_{kn} - \frac{2}{3}\delta_{ik}\delta_{nm}\right)\delta(x-x')\,. \tag{2.8}$$

Now consider a system in equilibrium, and allow for small perturbations away from equilibrium in v_k and $n \to n_o + \delta n$. The equation of fluid mechanics to first order in the perturbations are

$$\frac{\partial}{\partial t}(nv_k) + \frac{\partial}{\partial x_k}(T^{cl}_{ik} + \Xi_{ik}) = 0\,, \quad \partial_t n + n_0 \frac{\partial v^k}{\partial x^k} = 0\,. \tag{2.9}$$

The velocity can be decomposed into longitudinal and transverse parts satisfying

$$\nabla \cdot v_t(r,t) = 0\,, \quad \nabla \times v_l(r,t) = 0\,. \tag{2.10}$$

This is easiest to implement if we restrict quantities to depend only on one spatial coordinate, say the z coordinate, and time, e.g. $v_k = v_k(z,t)$. Then v_z corresponds to the longitudinal component and $v_{x,y}$ correspond to the transverse components of the fluid velocity. Note that the results using this choice would match the results found if we had not made any restrictions on the coordinate dependence.

Using these restrictions, one finds the following system of fluid dynamic equations: The linear form of the continuity equation yields

$$\frac{\partial n}{\partial t} + n_0 \nabla \cdot v_l = 0 \tag{2.11}$$

and momentum conservation yields the following system of equations

$$\frac{\partial}{\partial t} v_t - \frac{\eta_{\rm cl}}{n_0}\Delta v_t = -\frac{1}{n_0}\partial_z \Xi_{xz}\,, \quad n_0 \frac{\partial}{\partial t} v_l = -\nabla \delta P + \frac{4}{3}\eta_{\rm cl}\nabla(\nabla \cdot v_l) - \partial_z \Xi_{zz}\,. \tag{2.12}$$

The velocities can be solved for by taking a mixed Fourier-Laplace transform. For simplicity, we will consider the transverse velocity:

$$v_t = \frac{1}{n_0}\frac{-ik\Xi_{xz}}{-i\omega + \gamma k^2}\,, \tag{2.13}$$

where $\gamma = \eta_{\rm cl}/n$. The symmetric correlator is

$$\langle v^t_i v^t_j \rangle = \frac{2}{n_0^2}(\delta_{ij} - \frac{k_i k_j}{k^2})\frac{k^2 \langle (\Xi_{xz})^2 \rangle}{\omega^2 + \gamma^2 k^4} \tag{2.14}$$

Evaluating the noise term, we find $\langle (\Xi_{xz})^2 \rangle = \eta_{\rm cl} T$ and hence

$$\langle v^t_i v^t_j \rangle = \frac{2T}{n_0}(\delta_{ij} - \frac{k_i k_j}{k^2})\frac{\gamma k^2}{\omega^2 + \gamma^2 k^4}\,. \tag{2.15}$$

Repeating this process for the longitudinal velocity, the entire velocity-velocity correlator is found to be

$$\Delta_{ij}^{S} \equiv \langle v_i v_j \rangle = \frac{2T}{n_0}\left[\frac{k_i k_j}{k^2}\frac{\tilde{\gamma}\omega^2 k^2}{(\omega^2 - c^2k^2)^2 + (\tilde{\gamma}\omega^2 k^2)^2} + \left(\delta_{ij} - \frac{k_i k_j}{k^2}\right)\frac{\gamma k^2}{\omega^2 + \gamma^2 k^4}\right] \tag{2.16}$$

where $\tilde{\gamma} = \frac{4}{3}\gamma$. The first and second term are representative of sound and shear waves respectively. Note that this is the symmetric correlator, as indicated by the superscript S. Now let us calculate the retarded velocity-velocity correlator by using the classical fluctuation-dissipation theorem.

$$\chi''(\omega) = \frac{1}{2}\beta\omega C(\omega) \tag{2.17}$$

with $\beta = 1/T$ being the inverse temperature and

$$C_{ij}(t) = \langle A_i(t) A_j(0)\rangle_c = \langle \delta A_i(t) \delta A_j(0)\rangle \,. \tag{2.18}$$

This is the Kubo or relaxation function where the subscript c stands for cumulant or connected. In Fourier space $C_{ij}(\omega)$ is the symmetric correlator of the fluctuations.

To find the retarded correlator, we must examine the generalized susceptibility. It is related to the time derivative of the Kubo function by

$$\chi_{ij}(t) = -\beta\Theta(t)\dot{C}_{ij}(t) \tag{2.19}$$

where $\Theta(t)$ is a step-function. The generalized susceptibility χ can be identified as the retarded correlator. Utilizing the relation $\chi'' = \mathrm{Im}(\chi)$ and that χ is analytic in the upper half plane the retarded velocity correlation function is uniquely determined:

$$\Delta_{ij}^{R} = \frac{1}{n_o}\left[\frac{k_i k_j}{k^2}\frac{\omega^2}{(\omega^2 - c^2k^2)^2 + (i\omega k^2\tilde{\gamma})} + \left(\delta_{ij} - \frac{k_i k_j}{k^2}\right)\frac{-\gamma k^2}{-i\omega + \gamma k^2}\right] \tag{2.20}$$

The Kubo-Martin-Schwinger conditions relate the symmetric and retarded correlators in quantum mechanical regimes. In Fermi systems, the response functions are related to bosonic operators (e.g. bilinears of fermi operators). Therefore, a classical version of the KMS relation is found to be $G_s = \frac{2T}{\omega}\mathrm{Im}(G_R)$. This is exactly the classical fluctuation-dissipation theorem .

2.4 Contribution of Thermal Fluctuations

Finally, we have arrived at the precipice of our main goal. The effect of stochastically governed sound and shear waves can be calculated. As mentioned earlier, we will be interested in the retarded correlator between two stress tensors $G^R_{xyxy}(x-y) = \langle T_{xy}(x)T_{xy}(y)\rangle_R$. The symmetric correlator at vanishing external spatial momentum is

$$G_S^{xyxy}(\omega, k=0) = n^2 \int \frac{d\omega'}{2\pi} \int \frac{d^3\mathbf{p}}{(2\pi)^3} \Big(\Delta_S^{xx}(\omega', \mathbf{p})\Delta_S^{yy}(\omega-\omega', -\mathbf{p}) + \Delta_S^{xy}(\omega', \mathbf{p})\Delta_S^{yx}(\omega-\omega', -\mathbf{p}) \Big) \tag{2.21}$$

This assumes small, nearly linear hydrodynamic fluctuations and small frequencies [31]. The KMS relation, $G_s = \frac{2T}{\omega}\mathrm{Im}(G_R)$, could be used to find shear viscosity from the symmetric correlator. This is not practical, as τ_π is dependent on the retarded function. Therefore, we would have to invert the KMS relation by using a Kramers-Kronig relation in order to find the real part of G^R. Instead, it is more economical to compute G^R directly.

$$\begin{aligned} G^R_{xyxy}(\omega, 0) = n^2 \int \frac{d\omega'}{2\pi} \int \frac{d^3\mathbf{p}}{(2\pi)^3} \times \\ \Big(\Delta_S^{xx}(\omega', \mathbf{p})\Delta_R^{yy}(\omega-\omega', -\mathbf{p}) + \Delta_S^{xy}(\omega', \mathbf{p})\Delta_R^{yx}(\omega-\omega', -\mathbf{p}) + \\ \Delta_S^{xx}(\omega', \mathbf{p})\Delta_R^{yy}(\omega-\omega', -\mathbf{p}) + \Delta_S^{xy}(\omega', \mathbf{p})\Delta_R^{yx}(\omega-\omega', -\mathbf{p}) \Big) \end{aligned} \tag{2.22}$$

This expression, in the low frequency limit, reproduces G^s via the KMS relations.

We are now able to computer G^R. The calculation is done entirely within the hydrodynamic domain, therefore it is not accurate at large momentum. This is true for both G^R and the velocity propagators Δ^{ij}. Hence, we introduce a momentum cutoff at p_{max}, the largest momentum where hydrodynamics is applicable. The contribution of the first two shear-shear wave interactions after preforming the angular integrals is

$$\begin{aligned} G_R^{xyxy}(\omega, k=0) &= \frac{-7T}{30\pi^3}\int_0^{p_{max}} dp \int \frac{i\gamma^2 p^6}{(\omega-\omega'+i\gamma p^2)\ (\omega'^2+\gamma^2 p^4)} d\omega' \\ &= \frac{7T}{60\pi^2}\int_0^{p_{max}} \frac{-p^4}{p^2-(i\omega/2\gamma)} dp \\ &= \frac{7T}{60\pi^2}\int_0^{p_{max}} dp\Big(-p^2-\frac{i\omega}{2\gamma}+\frac{i\omega^2}{2\gamma\omega+4i\gamma^2p^2}+\dots\Big) \\ &= \frac{-7Tp_{max}^3}{180\pi^2} - i\omega\frac{7Tp_{max}}{120\gamma\pi} + (1+i)\omega^{3/2}\frac{7T}{480\pi\gamma^{3/2}}+\dots \end{aligned} \tag{2.23}$$

Doing this for the last two term shear-shear terms, as they have they same poles, and dropping the p_{max}^3 as it corresponds to the pressure, and therefore is not of interest, the total shear-shear contribution is found to be

$$G_{R,shear-shear}^{xyxy}(\omega) = -i\omega\frac{7Tp_{max}}{60\gamma\pi} + (1+i)\omega^{3/2}\frac{7T}{240\pi\gamma^{3/2}}+\dots \tag{2.24}$$

The first term is a positive contribution to shear viscosity. The imaginary component of the second is a frequency dependent reduction to the shear viscosity. As the second term vanish as $\omega \to 0$, there is no problem in defining the shear viscosity as the zero frequency limit of $\partial G_R^{xyxy}/\partial\omega$. The real part of the second term can be used to interpret the validity of the hydrodynamic regime. It has the same sign as the τ_π in Eq(2.4) but the wrong ω dependance. Thus, it can be interpreted as a correction to τ_π that diverges at small frequency signaling the breakdown in the validity of the hydrodynamic expansion at one-derivative order.

In the hydrodynamic regime, where $p_{max}\gamma_n \ll 1$, the sound term in the velocity correlators can be simplified.

$$\frac{\omega^2}{(\omega^2-c^2k^2)^2+(i\omega k^2\tilde{\gamma})} \approx \frac{\omega}{2}\left(\frac{1}{\omega+i\tilde{y}_n/2p^2-p/c^2}+\frac{1}{\omega+i\tilde{y}_n/2p^2+p/c^2}\right) \tag{2.25}$$

The ω' poles in Eq(2.22) are now simple and the integration is preformed via simple contours. The mixed shear sound term behaves as

$$\frac{-T}{5\pi^2}\int_{-p_{max}}^{p_{max}} \mathrm{d}p \frac{p^4}{p^2-3i(\omega-p/c^2)/5\gamma_n} = \frac{2T}{3\pi^2}\gamma_n^2 p_{max}^5 + i\frac{2\gamma_n T}{3\pi^2}\omega p_{max}^3 \tag{2.26}$$

The shear-sound contribution is suppressed compared to the shear-shear contribution by additional powers of $\gamma_n p_{max}$. The sound-sound correlator is straight forward to evaluate and contributes at the same level as the shear-shear contribution as well as containing terms suppressed by additional powers of $\gamma_n p_{max}$. Combining these results to leading order in $\gamma_n p_{max}$, the relevant contribution to viscosity is

$$\begin{aligned} G^R_{xyxy}(\omega \ll p_{\max}, |\mathbf{k}| = 0) = \text{constant} - i\omega \frac{17 T p_{max}}{120 \gamma \pi^2} \\ + (1+i)\omega^{3/2} \frac{(28+3\sqrt{6})T}{980 \pi \gamma^{3/2}} + \dots \end{aligned} \tag{2.27}$$

where $\gamma = \frac{\eta}{n}$ and $p_{\max}$ is the cut-off for the effective theory of hydrodynamics. The leading constant term is a renormalization of the pressure and does not affect transport, hence we will ignore it in the following. Note that terms not included in Eq. (2.27) are those that are suppressed by higher powers of $p_{\max}\gamma$, which is the "small parameter" of the effective theory. Similarly, higher loop contributions to G_R^{xyxy} are suppressed by higher powers of $p_{\max}\gamma$. Thus, up to first order in powers of $p_{\max}\gamma$, the result for the retarded correlator is given by the sum of the "classical" result Eq. (2.4) and the one-loop result Eq. (2.27).

As noted before, the $i\omega$ term is a contribution to the shear viscosity. This contribution is dependent on the momentum cutoff of p_{max}, but the physical viscosity must be independent of such an arbitrary cutoff. Therefore, the bare viscosity must be dependent on the cutoff as well, and its cutoff dependance is governed by a renormalization group equation. The non-analytic term, $\omega^{3/2}$, cannot be cutoff dependent because any dependence cannot be absorbed into the hydrodynamic parameters. This is required for the consistency of hydrodynamics as an effective theory.

2.5 Minimum on viscosity

In this section our main result, Eq(2.27), is used to find the physical viscosity. The viscosity is found using the Kubo relation

$$\eta = \lim_{\omega \to 0} \frac{-\text{Im} G^R_{xyxy}(\omega, \mathbf{k}=0)}{\omega}\,, \tag{2.28}$$

the result for the physical viscosity including fluctuations to first loop order is given by

$$\eta = \eta_{\rm cl} + \frac{17 T p_{\rm max} n}{120 \eta_{\rm cl} \pi^2} \,, \tag{2.29}$$

where again the index "cl" refers to "classical" contributions in the sense of turning off all fluctuations. As was previously noted, our calculation is systematic if

$$p_{\rm max} \ll \frac{n}{\eta_{\rm cl}} \,, \tag{2.30}$$

so we parametrize $p_{\rm max}$ by

$$p_{\rm max} = \frac{n}{\eta_{\rm cl}} \Phi \,,$$

where Φ is a dimensionless function of thermodynamic variables that should be small. For instance, we may take[2] Φ to be a function of pressure over density, $\Phi = \Phi(P/n)$. Then the result for the physical viscosity may be cast into a result for the dimensionless viscosity over density ratio,

$$\left(\frac{\eta}{n}\right) = \left(\frac{\eta}{n}\right)_{\rm cl} + \frac{17 T n^2 \Phi(P/n)}{120 n^3 \, (\eta/n)_{\rm cl}^2 \, \pi^2} \,.$$

This expression can be extremized. We find that the physical viscosity over density expression may never decrease below the minimum value

$$\left(\frac{\eta}{n}\right) \geq \left(\frac{\eta}{n}\right)_{\rm min} = \left(\frac{153 T n^2 \Phi(P/n)}{160 \pi^2 n^3}\right)^{1/3} \,. \tag{2.31}$$

The minimum value for viscosity is dimensionless and presumably universal, meaning that for a unitary Fermi gas it should only depend on the combination T/T_F, with $T_F = \frac{(3\pi^2 n)^{2/3}}{2m}$. Assuming a power-like behavior, we have

$$\left(\frac{153 T n^2 \Phi(P/n)}{160 \pi^2 n^3}\right) \propto \left(\frac{T}{T_F}\right)^{\alpha} \,,$$

with α a constant. Similarly, we take Φ to be given by a power law with behavior

$$\Phi(P/n) \propto (P/n)^{\beta} \,,$$

[2] In principle, Φ may also depend on the combination T/T_F with T_F the Fermi temperature. However, we will drop this dependence in favor of a constant that may vary around unity.

with β a constant. As shown in section 2.6 , the pressure is given by the relation $P = nTG(T/T_F)$ and $\lim_{T\to\infty} G = 1$. With this, we find

$$\frac{Tm^2}{n}\left(\frac{T}{m}\right)^{\beta} \propto \left(\frac{T}{T_F}\right)^{\alpha},$$

which leads to the requirement $\alpha = 1 + \beta$, $2 - \beta = \alpha$ and thus

$$\alpha = \frac{3}{2}, \quad \beta = \frac{1}{2}.$$

Thus, we obtain the final form of the lower viscosity bound

$$\left(\frac{\eta}{n}\right) \geq \left(\frac{\eta}{n}\right)_{\min} = \left(k\frac{153Tn^2\sqrt{P/n}}{160\pi^2 n^3}\right)^{1/3}, \tag{2.32}$$

with k an arbitrary constant of order unity. One finds

$$\left(\frac{\eta}{n}\right) \geq \left(\frac{\eta}{n}\right)_{\min} = \left(k\frac{459\sqrt{\frac{T^3}{T_F^3}\frac{P}{nT}}}{2^{3/2}160}\right)^{1/3} \simeq 1.005k^{1/3}\sqrt{\frac{T}{T_F}}\left(\frac{P}{nT}\right)^{1/6}, \tag{2.33}$$

which matches the result found in [14].

2.5.1 Calculating the classical viscosity

Given a liquid with a measurable energy-momentum tensor component T^{xy}, the shear viscosity of that liquid can be defined using the Kubo relation. Since this (physical) viscosity will in general differ from the classical viscosity η_{cl} we have defined above, this may cause some confusion. Thus we will take this as an opportunity to clarify how the two quantities will differ and point out an example of how to obtain both of these quantities.

Let us start by pointing out that the real, physical viscosity η of a system is what one obtains if one performs a measurement of the correlator G^R_{xyxy} from experiment and then uses Eq. (2.28) to obtain η. Similarly, if one was able to simulate a fully quantum non-equilibrium system and unambiguously extract the correlator from this simulation, the Kubo formula of this quantity would yield the physical shear viscosity. Since, at the time of writing, this is prohibited by the so-called sign problem, let us investigate what happens if one turns to the usual kinetic theory method to

extract the shear viscosity. For this purpose, consider a scalar quantum field with a quartic self-interaction with coupling constant λ. It is well known that in the limit of weak coupling $\lambda \to 0$. The dynamics of this quantum field is well approximated by kinetic theory (cf. [7]):

$$\partial_t f(\mathbf{p}, \mathbf{x}, t) + \frac{1}{E}\mathbf{p} \cdot \nabla f(\mathbf{p}, \mathbf{x}, t) = -\mathcal{C}[f]\,, \tag{2.34}$$

where $f(\mathbf{p}, \mathbf{x}, t)$ is the phase-space distribution of particles with momentum $\mathbf{p}$ and energy E, and $\mathcal{C}[f]$ is the collision kernel that is proportional to the transport cross section, $\mathcal{C}[f] \sim \lambda^2$. It is also well known that the description in terms of kinetic theory breaks down once the (quasi-)particle states start to have a width that is comparable to their mass, which typically happens when the coupling λ starts to become sizable.

Nevertheless, as long as $\lambda \ll 1$ the description in terms of kinetic theory is applicable, and one can use known techniques such as the Chapman-Enskog expansion or Grad's 14 moment method to extract the shear viscosity η_{KT} from the kinetic description. Normalizing by particle density, one finds

$$\frac{\eta_{KT}}{n} \sim \frac{1}{\lambda^2}\,,$$

up to logarithmic corrections in λ, and where we have suppressed dimensionful parameters that depend on the problem of interest (mass, temperature, etc.).

Now consider the contribution to the physical viscosity arising from hydrodynamic fluctuations, Eq. (2.29). If the coupling is weak, we expect kinetic theory to give a good description of the physical viscosity. Sound modes should be short-lived, and hence the contribution coming from fluctuating hydrodynamics should be small. Hence, we are led to identify

$$\eta_{\rm cl} \simeq \eta_{KT} + \mathcal{O}(\lambda^{-1})\,.$$

But if this is the case, one may ask the question of why the kinetic theory description misses the contribution to viscosity from fluctuations as the coupling strength λ is increased. Plugging in the above estimates one finds

$$\eta - \eta_{\rm cl} = \frac{17Tn^2}{120\eta_{\rm cl}^2\pi^2}\Phi \propto \lambda^4 T m^2 \Phi\,.$$

In other words, the fluctuating contribution to η is suppressed by six powers of the coupling strength λ with respect to η_{KT}. Clearly, the original kinetic description Eq. (2.34) with $\mathcal{C}[f] \propto \lambda^2$ is not accurate to this order in the coupling. Moreover, it is known that to capture effects at this order in the coupling constant, it would not even be sufficient to calculate the cross section or collision kernel $\mathcal{C}[f]$ correctly up to λ^6 because the kinetic theory description contains new structures that cannot be brought in the simple form of a Boltzmann equation, cf. [52].

To conclude, at weak coupling, a good approximation to the "classical" viscosity can be calculated microscopically by using a kinetic theory description. However, care must be taken in so far as this identification relies on properly calculating the weak coupling cross section used in the kinetic theory treatment. Furthermore, the kinetic theory description will become inaccurate as the coupling strength is increased, since the kinetic theory description cannot be systematically improved beyond the leading-order. Comparing the parametric dependence on the coupling λ, it is likely that η_{KT} will become an inaccurate approximation of $\eta_{\rm cl}$ before the physical viscosity is dominated by the contribution arising from fluctuations, e.g. at intermediate values of the coupling strength.

2.5.2 Determination of Systematic Expansion?

One may worry if the expansion based on Eq. (2.30) is systematic because, at first glance, both $p_{\rm max}$ as well as $n/\eta_{\rm cl}$ are expected to scale as the inverse mean free path. In the case at hand, however, we found that $p_{\rm max}$ is equal to $n/\eta_{\rm cl}$ times a dimensionless function $\Phi = \sqrt{P/n}$. Our setup is thus systematic, as long as

$$\Phi \sim \frac{1}{v}\sqrt{\frac{k_B T}{m}} \sim \frac{c_T}{c} \ll 1\,,$$

where c_T is the thermal speed of the atoms. Note that we have restored standard units and included a characteristic system-dependent speed v that is needed to make Φ dimensionless, as required. In a relativistic system, v would simply be the speed of light. Since the speed of light does not arise in our non-relativistic treatment, we have to construct another characteristic speed that must not

depend on the temperature or on the particle masses (otherwise the resulting function Φ would not satisfy the scaling requirement outlined in the beginning of this section). We are thus forced to construct a characteristic speed out of the typical system size $L \sim 100\mu m$ and the period $t = 2\pi/\omega$ from the trapping frequency $\omega \simeq 2\pi \times 2000$ Hz (cf. [2]), finding $v \simeq 0.5$ m/s. The typical temperatures considered are on order the Fermi temperature

$$T_F \simeq \frac{\hbar}{k_B}\omega(6N)^{1/3}\,,$$

where the number of atoms is typically $N \simeq 7.5 \times 10^4$, hence $T_F \simeq 7.9\mu K$ and thus, for a cold quantum gas of Li^6 atoms, $c_T \simeq 0.1$ m/s. Hence we find

$$\Phi = \frac{c_T}{v} \simeq 0.2\,,$$

which is sufficiently small to suggest that higher order corrections are suppressed, but not so different from unity as to put our earlier estimate for the constant $k \simeq 1$ in Eq(2.33) into question. To conclude, for temperatures on the order of T_F there seems to be a small parameter, Φ, allowing the expansion in powers of fluctuations to be systematic, but we do expect sizable corrections to our leading order result. Therefore, we expect our results based on a leading order analysis to be qualitatively robust, but not quantitatively accurate.

2.6 Equation of State

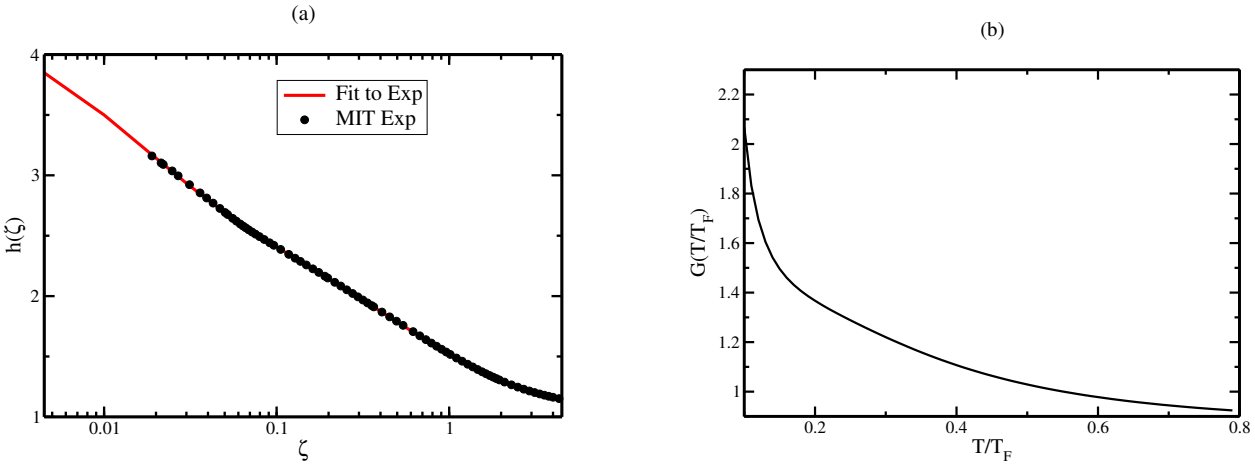

Figure 2.2: Left: results for the normalized pressure P/P_0 from the MIT experiment [32] and a 5 parameter fit (see text for details). Right: The function $G = \frac{P}{nT}$ as a function of T/T_F.

The lower bound on viscosity, Eq(2.33), is dependent on the thermodynamics properties of the fluid. Therefore, in this section a practical form for the evaluation of the equation of state is found, enabling us to compare our bound with experimental data.

The equation of state of a cold unitary Fermi gas was measured experimentally by the MIT group [32]. The result from [32] for the pressure (versus fugacity $\zeta = e^{-\mu/T}$) is shown in Fig(2.2.a). The result for the pressure is normalized by the ideal non-interacting single-component Fermi gas pressure,

$$P_0(\mu, T) = -T\lambda_{dB}^{-3}\mathrm{Li}_{5/2}(-\zeta^{-1})\,,$$

where $\lambda_{dB} = \sqrt{\frac{2\pi}{mT}}$ is the deBroglie wavelength. Also shown in Fig(2.2.a) is a fit of the experimental data using the parametrization

$$h(\zeta) \equiv P(\mu, T)/P_0(\mu, T) = \frac{\zeta^3 + c_1\zeta^2 + c_2\zeta + c_3}{\zeta^3 + c_4\zeta^2 + c_5\zeta + 1}$$

which is a variant of the approach followed in [45]. A least squares fit gives

$$c_1 = 101.591\,, \quad c_2 = 158.375\,, \quad c_3 = 4.30128\,, \quad c_4 = 104.884\,, \quad c_5 = 67.3894\,.$$

Note that c_3 is related to the Bertsch parameter ξ as $c_3 = \xi^{-3/2}$ from the relation $P(\mu, T = 0) = \xi^{-3/2} P_0(\mu, T = 0)$. The fitted value of c_3 therefore corresponds to $\xi = 0.378$. Using the thermodynamic relation $n = \frac{\partial P}{\partial \mu}\Big|_T$ and the identity $n = \lambda_{dB}^{-3} \frac{(4\pi)^{3/2}}{3\pi^2} \left(\frac{T_F}{T}\right)^{3/2}$, one has

$$\frac{(4\pi)^{3/2}}{3\pi^2} \left(\frac{T_F}{T}\right)^{3/2} = \zeta \frac{\partial}{\partial \zeta} \left(\mathrm{Li}_{5/2}(-\zeta^{-1}) h(\zeta) \right) ,$$

and hence a (numerical) result for $\zeta = \zeta(T/T_F)$ by inverting the above functional relation.

Using the above relations, the pressure may be written as

$$P(\mu, T) = nTG(\zeta) , \quad G(\zeta) = \frac{1}{-\zeta \frac{d}{d\zeta} \ln \left[-\mathrm{Li}_{5/2}(-\zeta^{-1}) h(\zeta) \right]} .$$

For convenience, the function G is plotted in Fig(2.2.b) as a function of T/T_F. As can be seen, the form of G implies that the pressure is close to nT, but not monotonically larger or smaller than nT in the domain considered. We have checked that $\lim_{T\to\infty} G(T/T_F) \to 1$, as expected.

From our parameterization, we can calculate thermodynamic quantities. For example, the compressibility can be calculated by $\kappa = \frac{1}{n^2} \frac{\partial^2 P}{\partial \mu^2}|_T$. As the compressibility is dependent on the second derivative of the pressure, it contains a clear signature of the superfluid λ phase transition Ref. [32]. Another thermodynamic quantity of interest is the entropy s. This can be calculated from $s = \frac{\partial P}{\partial T}|_\mu$ or from $s/Nk_B = \frac{T_F}{T}(\frac{P}{P_0} - \frac{\mu}{E_F})$, where E_F is the Fermi energy. In Fig(2.3) thermodynamic quantities found though manipulation of our fitted function are compared to experimental data. The error is generally less the two percent, and increases as the number of derivatives increases and in the high $\beta\mu$ regime. This is not problematic as we are most interested in the low $\beta\mu$ regime.

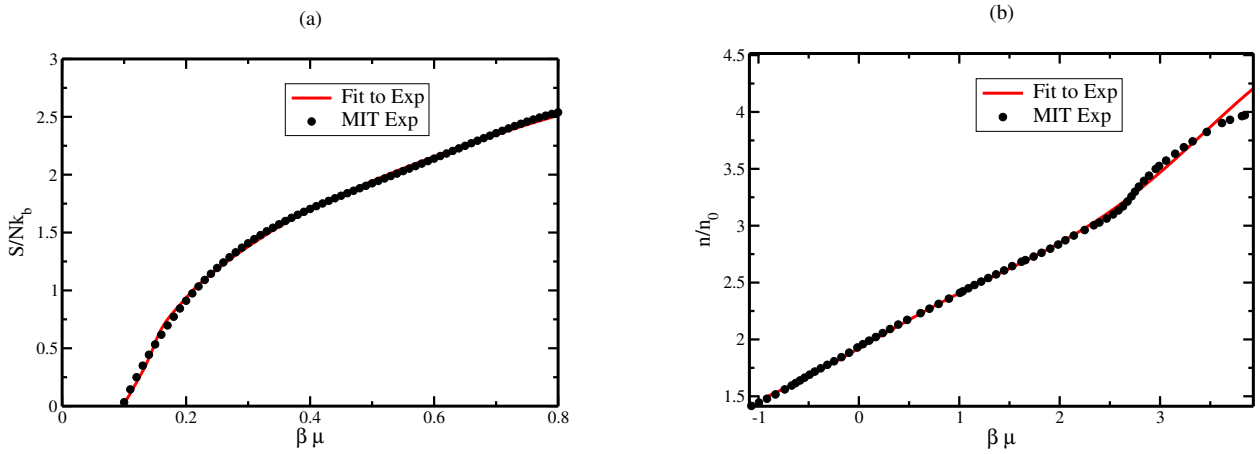

Figure 2.3: Left: The entropy per particle as a function of $\beta\mu$ where $\beta = 1/(k_B T)$ Right: The density of a unitary fermi gas normalized by the density of a non-interacting fermi gas at the same chemical potential μ and temperature T. The red line is the thermodynamic quantity found through manipulation of our fitted function Eq(2.6).

2.7 Discussion and Conclusion

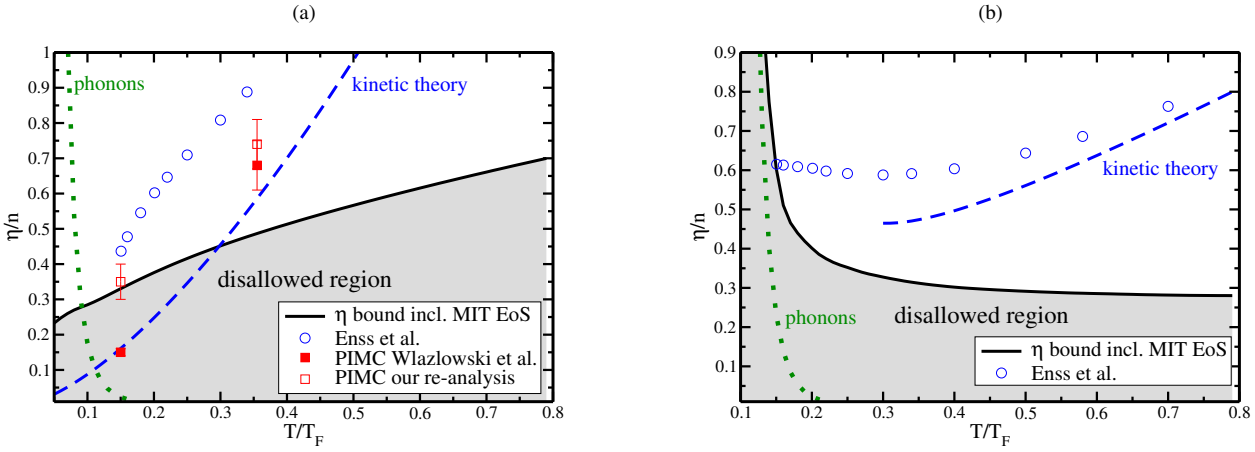

Figure 2.4: Summary of results for η/n (left) and η/s (right). The viscosity limit from Eq. (2.33) was used to delineate a "disallowed region" of viscosity values using the MIT equation of state from [32] for P/nT and S/N and the estimate $k = 1$. Also shown are results from kinetic theory at high temperatures and the phonon scattering at low temperatures (see text for details), as well as results from Enss et al., [20]. Furthermore, we indicate the results from the PIMC calculation by Wlazlowski et al. [53] and our own re-analysis of the same data (see [42] for a discussion of the re-analysis). Note that the resulting value for η/n is consistent with the "upper bound" reported in the supplement to [53].

Employing the framework of hydrodynamics in the presence of fluctuations, the low frequency behavior to the shear viscosity spectral function has been calculated. The calculation gives a bound on the physical shear viscosity, Eq. (2.33), which matches the result found in [14]. The situation is summarized in Fig(2.4), where the viscosity bound Eq. (2.33) is shown together with the viscosity in kinetic theory (cf. Ref [37])

$$\left.\frac{\eta}{n}\right|_{KT} = \frac{45\pi^{3/2}}{32\times 2^{3/2}}\left(\frac{T}{T_F}\right)^{3/2} \simeq 2.768\left(\frac{T}{T_F}\right)^{3/2} \tag{2.35}$$

as well as the viscosity of (inelastic) phonon scattering in the superfluid phase, (cf. Ref [36, 8])

$$\frac{\eta}{n}\Big|_{phonons} = \frac{\eta}{s}\Big|_{phonons}\frac{s}{n} \simeq 1.18\times 10^{-7}\left(\frac{T_F}{T}\right)^5 . \tag{2.36}$$

Also shown in Fig(2.4) are results for the minimum η/s, using the experimental data from [32] for the entropy per particle as a function of temperature. The corresponding results for kinetic theory and phonons are [43, 48, 36]

$$\frac{\eta}{s}\Big|_{KT} = 2.768\left(\frac{T}{T_F}\right)^{3/2}\frac{1}{\frac{5}{2}+\ln\left[\frac{3\sqrt{\pi}}{4}(T/T_F)^{3/2}\right]}, \quad \frac{\eta}{s}\Big|_{phonons} = 4\times 10^{-9}\left(\frac{T_F}{T}\right)^8 . \tag{2.37}$$

One observes that the viscosity result from kinetic theory enters the disallowed region at around $T/T_F \lesssim 0.3$. We interpret this as meaning that kinetic theory loses its validity at or below this temperature. Similarly, the viscosity result from the superfluid analysis enters the disallowed region for $T/T_F \sim 0.1$. Again, we interpret this as meaning that the calculation loses validity at or below this temperature. The results for the shear viscosity by Enss et al. stay within the allowed region for all temperatures shown, but it is interesting to note that the η/s values at low temperatures stop at the boundary to the disallowed region.

We conclude that the theory of hydrodynamic fluctuations can provide a relevant tool to study the properties of unitary Fermi gases. Specifically, we expect that our findings may help in the analysis of future quantum Monte Carlo calculations. We plan to further develop this theory in the future.

Chapter 3

Lattice Boltzmann

3.1 Introduction

In this chapter various lattice Boltzmann schemes will be derived and discussed. Lattice Boltzmann schemes are popular methods for fluid dynamics simulation. The absence of the non-linear advection term present in the Navier-Stokes equation and ease of parallel computation have made these methods popular. We will be using theses schemes to simulate the elliptic flow observed in unitary fermi gasses. This is discussed in detail in the next section. The mesoscopic approach of the lattice Boltzmann equation should do well in the lower density outer edge of the cold atom clouds where traditional fluid mechanics may suffer. Three different lattice Boltzmann methods will be developed and tested. The development of kinetic theory and the isothermal lattice Boltzmann model (ILB) will largely follow Succi's book [51]. The Taylor expansion thermal lattice Boltzmann (TLB) first developed by He, Chen and Doolen in 1998 presentation will roughly follow the original paper [25]. Lastly, the Hermite projection based expansion thermal lattice Boltzmann model (HLB) will follow the 2010 work of Hung [28].

3.1.1 Kinetic Theory

The Boltzmann equation governing the single particle distribution function of a single component fluid is

$$\partial_t f + (\xi \cdot \nabla) f = \Omega(f) \tag{3.1}$$

where $f(x,t,\xi)$ is the distribution function, ξ is the particle velocity, Ω is a collision term, and x and t are the space and time coordinates respectively. This equation governs momentum transport in the fluid. This is the balance of free streaming particles, where a particle's trajectory is unchanging, and collisions, where a scattering events occur. Macroscopic variables can be calculated as moments of the distribution function.

$$\begin{aligned} \rho &= \int f \ d\xi \\ \rho u &= \int \xi f \ d\xi \\ \frac{\rho D R T}{2} &= \int \frac{(\xi - u)^2}{2} f \ d\xi \end{aligned} \tag{3.2}$$

where ρ is the density and u is the bulk fluid velocity. The dimension of the system is D, and R is the gas constant. The collision term is a complicated term involving the integral over momentum space of single particle distribution functions and scattering probability functions. For simplicity, a Bhatnagar, Gross and Krook (BGK) simplification for the collision term will be used.

$$\Omega(f) = -\frac{f - f_{eq}}{\tau} \tag{3.3}$$

where τ is the relaxation time and f_{eq} is the equilibrium distribution function given by the Maxwell-Boltzmann equation

$$f_{eq} = \frac{\rho}{(2\pi RT)^{D/2}} \exp\left[\frac{(\xi - u)^2}{2RT}\right] \tag{3.4}$$

It is well known that by using a Chapman-Enskog expansion the Boltzmann-BGK equation reproduces the familiar continuity and momentum equations at the Navier-Stokes level.

$$\begin{aligned} &\partial_t \rho + \nabla \cdot (\rho u) = 0 \\ &\rho(\partial_t u + u \cdot \nabla u) = -\nabla p + \nabla \cdot \Pi \\ &\Pi = \rho\nu(\nabla u + u\nabla) \end{aligned} \tag{3.5}$$

where Π is the viscous stress tensor. The pressure is that of an ideal gas, $p = \rho RT$, and the relaxation time is related to the viscosity $\nu = \tau RT$. At this point one can follow the standard derivation of the lattice Boltzmann equation. The disadvantage is that the resulting algorithm will be isothermal, and therefore not account for temperature dependent effects.

To allow for temperature dependence we introduce the internal energy density distribution function.

$$g = \frac{(\xi - u)^2}{2} f \tag{3.6}$$

The internal energy density distribution function, g, has been chosen such that the integral over velocity space gives the internal energy density $\rho\epsilon$, where $\epsilon = DRT/2$. At first glance, it appears that this is not necessary as it is simply related to f. This function is introduced to allow for the freedom to solve a nontrivial energy equation that controls the temperature distribution. The governing evolution equation is

$$\begin{aligned} \partial_t g + (\xi \cdot \nabla) g &= \frac{(\xi - u)^2}{2} \Omega(f) - fq \\ q &= (\xi - u) \cdot (\partial_t u + (\xi \cdot \nabla) u) \end{aligned} \tag{3.7}$$

The q term accounts for viscous heating. The collision term is given by a BGK approximation, and the equilibrium distribution is given by the Maxwell-Boltzmann equation.

$$\begin{aligned} \frac{(\xi - u)^2}{2} \Omega(f) &= \frac{g - g_{eg}}{\tau_c} \\ g_{eq} &= \frac{\rho (\xi - u)^2}{(2\pi RT)^{D/2}} \exp\left[\frac{(\xi - u)^2}{2RT}\right] \end{aligned} \tag{3.8}$$

The momentum equation Eq(3.1), and the energy equation Eq(3.7) govern the fluid flow and account for viscous dissipation and compression work. External forces can be added by including additional terms, but are omitted for simplicity [25].

3.1.2 Discretization of the Particle Distribution Function

In this section, the isothermal lattice Boltzmann equation (ILB) will be derived. This method contains a single distribution function f. Therefore, we will currently only be concerned with the momentum equation. A set of discrete velocities, ξ_α, will be found by forcing the moments, Eq(3.2), to be exactly reproduced. The spacial and time derivatives will be approximated by standard finite element methods. In most of the previous LBE models, the collision operator in the Boltzmann-BGK equation was assumed constant during each time step. This assumption introduces a second-order truncation error in the lattice Boltzmann equation. For the LBE isothermal model, this truncation error can be totally absorbed into the physical viscosity term. The only effect is a change of the viscosity from $\eta = \tau RT$ to $\eta = (\tau - 0.5\delta_t)RT$.

For a thermal model, this truncation is no longer trivial and will be addressed in the next section. The complication is due to the viscosity being present in both the momentum and energy equations. Specifically, the viscous heat dissipation term in the energy equation is a result of the non-equilibrium component of the density distribution. The viscosity term is not effected by the second order Chapman-Enskog expansion. This results in the viscous heat dissipation term involving viscosity $\eta = \tau RT$, not $(\eta = \tau - 0.5\delta_t)RT$ as needed for consistency. This inconsistency is the difficulty that must be dealt with when deriving thermal LBE. Initially, we integrate the particle distribution function using a second order strategy.

$$\begin{aligned} f(x+\xi\delta_t, \xi, t+\delta_t) - f(x,\xi,t) = \\ -\frac{\delta_t}{2\tau_c}[f(x+\xi\delta_t,\xi,t+\delta_t) - f_{eq}(x+\xi\delta_t,\xi,t+\delta_t)] \quad -\frac{\delta_t}{2}[f(x,\xi,t) - f_{eq}(x,\xi,t)] \end{aligned} \tag{3.9}$$

The left hand side is the result from the integration of the material derivative, $\partial_t + (\xi \cdot \nabla)$. In order to make the equations explicit, we redefine the variable f.

$$f \equiv f + \frac{\delta_t}{\tau + 0.5\delta_t}(f - f_{eq}) \tag{3.10}$$

This leads to an evolution equation of

$$f(x+\xi\delta_t,\xi,t+\delta_t)-f(x,\xi,t)=-\frac{\delta_t}{\tau+0.5\delta_t}[f(x,\xi,t)-f_{eq}(x,\xi,t)] \tag{3.11}$$

Now the velocity space must be discretized. It has been shown that to recover the continuity and momentum equations at the continuum Navier-Stokes level, the zeroth through third moments of the equilibrium distribution function, Eq(3.2), must be exact [25]. Taylor expanding the Maxwell-Boltzmann equilibrium distribution function to second order in u, we have

$$\begin{aligned} f_{eq} &= \frac{\rho}{(2\pi RT)^{D/2}}\exp\left[\frac{(\xi-u)^2}{2RT}\right]\approx \\ &(2\pi)^{-D/2}\rho(RT)^{-D/2}e^{-\frac{\xi^2}{2RT}}+\frac{(2\pi)^{-D/2}\xi\rho u(RT)^{-D/2}e^{-\frac{\xi^2}{2RT}}}{RT} \\ &-\frac{2^{-\frac{D}{2}-1}\pi^{-D/2}\rho u^2(RT)^{-D/2}e^{-\frac{\xi^2}{2RT}}\left(RT-\xi^2\right)}{R^2T^2}+O\left(u^3\right) \end{aligned} \tag{3.12}$$

The above criterion require that the integral below be exact up to third order, $m=0,1,\ldots 3$.

$$\int \xi^m f_{eq}(\xi)\ \mathrm{d}^D\xi=\sum_\alpha w_\alpha f_{eq}(\xi_\alpha) \tag{3.13}$$

where D is the number of dimensions. This ensures that the macroscopic variables are precisely found. In two dimensions this is accomplished by using a third order Gauss-Hermite quadrate. This leads to a nine discrete velocities.

$$\xi_\alpha=\begin{cases} (0,0) & \alpha=0 \\ c\Big(\cos(\frac{\pi}{2}(\alpha-1)),\ \sin(\frac{\pi}{2}(\alpha-1))\Big) & \alpha=1,2,3,4 \\ c\sqrt{2}\Big(\cos(\frac{\pi}{2}(\alpha-5)+\frac{\pi}{4}),\ \sin(\frac{\pi}{2}(\alpha-5)+\frac{\pi}{4})\Big) & \alpha=5,6,7,8 \end{cases} \tag{3.14}$$

The speed of sound is given by $c=\sqrt{3RT}$, and is generally taken to be $c=\sqrt{3}$. The discrete density distribution function is governed by the evolution equation

$$f_\alpha(x+e_\alpha\delta_t,t+\delta_t)-f_\alpha(x,t)=-\frac{\delta_t}{\tau+0.5\delta_t}[f_\alpha(x,t)-f_\alpha^{eq}(x,t)] \tag{3.15}$$

The Taylor expanded equilibrium distribution function is evaluated with the discrete velocities and truncation at second order.

$$f_\alpha^{eq} = w_\alpha \rho \left(1 + 3\frac{e_\alpha \cdot u}{c^2} + 4.5\frac{(e_\alpha \cdot u)^2}{c^4} - 1.5\frac{u^2}{c^2} \right) \tag{3.16}$$

The weights are $w_0 = 4/9,\ w_{1,2,3,4} = 1/9$, and $w_{5,6,7,8} = 1/36$. The calculation of macroscopic variables, Eq(3.2), is accomplished via finite sums. This is an isothermal lattice Boltzmann scheme (ILB), defined by Eq(3.15) and Eq(3.16).

3.1.3 Thermal Lattice Boltzmann

When the Boltzmann equation is properly discretized in the temporal and velocity spaces, so that the resulting discrete equation satisfies the mass, momentum, and energy conservation at the Navier-Stokes level, the previous discrete scheme is exactly the lattice Boltzmann equation for isothermal flow. The same procedure can be applied to the Boltzmann energy equation. Care must be taken so that the physical viscosity is consistent between the momentum and energy equations. The resulting discrete scheme will serve as the thermal lattice Boltzmann equation which describes the evolution of the macroscopic temperature field. This section follows the work of He, Chen and Doolen [25].

Using the second-order temporal integration scheme, we integrate the Boltzmann energy equation, in one time step.

$$\begin{aligned} g(x+\xi\delta_t, \xi, t+\delta_t) - g(x,\xi,t) = \\ -\frac{\delta_t}{2\tau_c}[g(x+\xi\delta_t,\xi,t+\delta_t) - g_{eq}(x+\xi\delta_t,\xi,t+\delta_t)] \\ -\frac{\delta_t}{2} f(x+\xi\delta_t,\xi,t+\delta_t) q(x+\xi\delta_t,\xi,t+\delta_t) \\ -\frac{\delta_t}{2}[g(x,\xi,t) - g_{eq}(x,\xi,t)] - \frac{\delta_t}{2} f(x,\xi,t) q(x,\xi,t) \end{aligned} \tag{3.17}$$

To make the equations explicit, we redefine the distribution function g.

$$g \equiv g + \frac{\delta_t}{2\tau_c}(g - g_{eq}) + \frac{\delta_t}{2} f q \tag{3.18}$$

The evolution equation for the new variable is

$$g(x+\xi\delta_t,\xi,t+\delta_t)-g(x,\xi,t)= \\ -\frac{\delta_t}{\tau_c+0.5\delta_t}[g(x,\xi,t)-g_{eq}(x,\xi,t)]-\frac{\delta_t}{\tau_c+0.5\delta_t}f(x,\xi,t)q(x,\xi,t) \tag{3.19}$$

Now the particle velocity space must be discretized. Ideally, it will be possible to use the same discretization for both the mass and energy density distributions functions, f and g. To accomplish this, the equilibrium distribution function, g_{eq}, is Taylor expanded up to order u^2

$$g_{eq}=\frac{\rho\epsilon}{(2\pi RT)^{2/D}}\exp\left(-\frac{\xi^2}{2RT}\right)\left[\frac{\xi^2}{DRT}+\left(\frac{\xi^2}{DRT}-\frac{2}{D}\right)\frac{\xi\cdot u}{RT}+ \\ \left(\frac{\xi^2}{DRT}-\frac{4}{D}\right)\frac{(\xi\cdot u)^2}{2(RT)^2}-\left(\frac{\xi^2}{DRT}-\frac{2}{D}\right)\frac{u^2}{2RT}\right] \tag{3.20}$$

The recovery of the macroscopic energy equation involves the zeroth through second order moments of the equilibrium internal energy distribution function, Eq(3.20) [25]. As the Taylor expanded internal energy distribution function is fourth order in ξ, a sixth order quadrature will be needed. Thus, the third order quadrature used in the previous section for the isothermal lattice Boltzmann is no longer valid.

This problem can be avoided if the terms are rewritten in such a way that the zeroth through second order moments of the second term vanish.

$$g_{eq}=\frac{\rho\epsilon}{(2\pi RT)^{2/D}}\exp\left(-\frac{\xi^2}{2RT}\right)\left[\frac{\xi^2}{DRT}+\left(\frac{\xi^2}{DRT}-\frac{2}{D}\right)\frac{\xi\cdot u}{RT}+\frac{(\xi\cdot u)^2}{2(RT)^2}-\frac{u^2}{2RT}\right] \\ +\frac{\rho\epsilon}{(2\pi RT)^{2/D}}\exp\left(-\frac{\xi^2}{2RT}\right)\left[\left(\frac{\xi^2}{DRT}+\frac{D+4}{D}\right)\frac{(\xi\cdot u)^2}{2(RT)^2}-\left(\frac{\xi^2}{DRT}-\frac{D+2}{D}\right)\frac{u^2}{2RT}\right] \tag{3.21}$$

Therefore, it can be discarded without effecting the recovery of the macroscopic quantities. There are multiple groupings to accomplish this goal, making this derivation somewhat unsatisfactory [24]. The freedom in the groupings results from the symmetry necessary to make the moments vanish. In section 3.1.4 this arbitrary is avoid through projection onto a Hermite polynomial basis. The zeroth through second order moments of Eq(3.21) only involve the zeroth- through fifth-order moments of Eq(3.13). Therefore, the same third order Gauss-Hermite quadrature, as used for the ILB, Eq(3.14), can be used, leading to a model with nine discrete speeds.

$$
\begin{aligned}
g_0^{eg} &= -\frac{2\rho\epsilon u^2}{3c^2} \\
g_{1,2,3,4}^{eq} &= \frac{\rho\epsilon}{9}\left(1.5 + 1.5\frac{e_\alpha \cdot u}{c^2} + 4.5\frac{(e_\alpha \cdot u)^2}{c^4} - 1.5\frac{u^2}{c^2}\right) \\
g_{5,6,7,8}^{eq} &= \frac{\rho\epsilon}{36}\left(3 + 6\frac{e_\alpha \cdot u}{c^2} + 4.5\frac{(e_\alpha \cdot u)^2}{c^4} - 1.5\frac{u^2}{c^2}\right)
\end{aligned}
\tag{3.22}
$$

The macroscopic internal energy integral can now be expressed as the following sum

$$
\rho\epsilon = \sum_\alpha (g_\alpha - \frac{\delta_t}{2} f_\alpha q_\alpha) \tag{3.23}
$$

The evolution equation for the internal energy distribution function is

$$
\begin{aligned}
&g_\alpha(x + e_\alpha\delta_t, t + \delta_t) - g_\alpha(x,t) = \\
&\quad - \frac{\delta_t}{\tau_c + 0.5\delta_t}[g_\alpha(x,t) - g_\alpha^{eq}(x,t)] - \frac{\delta_t}{\tau_c + 0.5\delta_t} f_\alpha(x,t) q_\alpha(x,t)\delta_t \\
&f_\alpha = \frac{\tau f_\alpha + 05\delta_t f_\alpha^{eq}}{\tau + 0.5\delta_t} \\
&q_\alpha = (e_\alpha - u)\cdot\left[\frac{1}{\rho}(-\nabla p + \nabla\cdot\Pi) + (e_\alpha - u)\cdot\nabla u\right]
\end{aligned}
\tag{3.24}
$$

The weakness of this method is that it is limited to the Boussinesq approximation [24]. That is the equation of state is $p = \rho R T_0$ where T_0 is a fixed reference temperature. The fixing of the temperature is required as it appears in the abscissas of the Gauss-Hermite quadrature, where a local variable is not permitted. The equilibrium distribution function is Taylor expanded to second order in u, below.

$$
g_{eq} \equiv \omega(\xi, T)\rho\left[\frac{\xi^2}{DRT} + \left(\frac{\xi^2}{DRT} - \frac{2}{D}\right)\frac{\xi\cdot u}{RT} + \frac{(\xi\cdot u)^2}{2(RT)^2} - \frac{u^2}{2RT}\right] \tag{3.25}
$$

where $\omega(\xi,T) = \frac{\rho\epsilon}{(2\pi RT)^{2/D}}\exp\left(-\frac{\xi^2}{2RT}\right)$. Evaluation of the quadrature $\int \omega(\xi,T) g_{eq}(\xi)\mathrm{d}\xi = \sum_\alpha w_\alpha g_{eq}(\xi_\alpha)$ will only result in constant weights, w_α, once the temperature is fixed. The speed of sound is fixed by the reference temperature to be $c^2 = RT_0$. This is the Taylor expansion lattice Boltzmann scheme for thermal flows (TLB). In the equilibrium distribution functions for f and g, Eq(3.16) and Eq(3.25), the temperature must be fixed. Once the temperature is fixed there is

no explicit coupling between the energy, Eq(3.24), and momentum, Eq(3.15), equations. Coupling can be introduce when the relaxation times, τ_c and τ, are dependent on temperature or density. If the relaxation time is taken to be independent of temperature, the evolution of the density and velocity fields will be identical to the values given by the ILB.

3.1.4 A Coupled Thermal Lattice Boltzmann Model

The Taylor expansion based thermal lattice Boltzmann method leaves much to be desired for the simulation of thermal flows. The model is limited to Boussinesq flows, where the temperature variations are small as the weights, $\omega(\xi_\alpha, T_0)$, must fixed at a reference temperature. As noted before, there are arbitrary choices made in determining the internal energy distribution function. A further complication is the q_α term that involves spacial gradients of pressure and velocity. These gradients add computational difficulty and decrease numerical stability. To avoid these shortfalls we develop a third method, expanding both the momentum and energy equations in the Hermite basis. Subsections 3.3.4-3.3.6 closely follows the work of Hung and Yang [28].

3.1.5 Moments and Truncated Hermite Series

Now we begin with the momentum equation and the total energy equation with a BKG collision term.

$$\begin{aligned} \partial_t f + (\xi \cdot \nabla) f &= -\frac{1}{\tau_f}(f - f_{eq}) \\ \partial_t h + (\xi \cdot \nabla) h &= -\frac{1}{\tau_g}(h - h_{eq}) + \frac{Z}{\tau_{hf}}(h - h_{eq}) \end{aligned} \tag{3.26}$$

where the equilibrium distribution functions are given by

$$\begin{aligned} f_{eq} &= \frac{\rho}{(2\pi RT)^{D/2}} \exp\left[-\frac{v^2}{2RT} \right] \\ h_{eq} &= \frac{\rho \xi^2}{2(2\pi RT)^{D/2}} \exp\left[-\frac{v^2}{2RT} \right] \end{aligned} \tag{3.27}$$

The total energy equation governs the evolution go of h, where $h = \xi^2 f/2$, and $\rho\epsilon = \int h \mathrm{d}\xi - \rho u^2/2$. Here, $v = \xi - u$, $\tau_{hf}^{-1} = \tau_f^{-1} = \tau_g^{-1}$, and $Z = \xi \cdot u - u^2/2$. Through the Chapman-Enskog expansion

of the two relaxation time kinetic model equations, the thermal hydrodynamic equations at the compressible Navier-Stokes level can be obtained.

$$\begin{aligned} \partial_t \rho + \nabla \cdot (\rho u) &= 0 \\ \partial_t (\rho u) + \nabla \cdot (\rho u u) &= -\nabla p + \nabla \cdot \Pi \\ \partial_t (\rho E) + \nabla \cdot [(p + \rho E) u] &= \nabla(\kappa) + \nabla \cdot (\Pi \cdot u) \end{aligned} \tag{3.28}$$

where the viscous stress tensor is $\Pi = \nu[\nabla u + (\nabla u)^T - (2/D)(\nabla \cdot u)I]$. The transport coefficients are related through the Chapman-Enskog expansion.

$$\nu = \tau_f p \qquad \kappa = c_v \tau_g P \qquad c_p = \frac{(D+2)R}{2} \tag{3.29}$$

The Prandtl number can be tuned arbitrarily by adjusting the relaxation times, $Pr = \gamma \tau_f / \tau_g$. The equation of the state is $p = \rho R T$. The temperature used, T, is the average of the temperatures found from the two distribution functions, T_f and T_h, found from the moments of their respective fields. This averaging provides good numerical stability and enables explicit coupling between the momentum and energy transport equations. The difference between the temperatures approaches zeros when a steady state solution is achieved.

$$\frac{D\rho R T_f}{2} = \int c^2 f \mathrm{d}\xi \qquad \frac{D\rho R T_h}{2} = \int h \mathrm{d}\xi - \frac{\rho u^2}{2} \tag{3.30}$$

To accommodate large temperature variations the equilibrium particle and internal energy distribution functions are expanded in a Hermite polynomial basis. As summarized in [28], there are three possible Hermit basis. We will follow Shat *et al* [49] .

We expand the distribution function in the dimensionless orthonormal Hermite (Gram-Charlier) polynomial basis in velocity space.

$$f(x, \xi, t) = \omega(\xi) \sum_{n=0}^{\infty} \frac{1}{n!} a^{(n)}(x, t) H^{(n)}(\xi) \tag{3.31}$$

where both $a^{(n)}$ and $H^{(n)}$ are rank-n tensors and the product on the right hand side is fully contracted. The coefficients are given by

$$a^{(n)}(x,t) = \int f(x,\xi,t)H^{(n)}(\xi)\ \mathrm{d}\xi \tag{3.32}$$

The coefficients are found to be related to the hydrodynamic moments.

$$\begin{aligned} a^{(0)} &= \int f \mathrm{d}\ \xi = \rho \\ a^{(1)} &= \int f\xi\ \mathrm{d}\xi = \rho u \\ a^{(2)} &= \int f(\xi^2 - \delta)\ \mathrm{d}\xi = P + \rho(u^2 - \delta) \\ a^{(3)} &= \int f(\xi^3 - \xi\delta)\ \mathrm{d}\xi = Q + ua^{(2)} - (D-1)\rho u^3 \end{aligned} \tag{3.33}$$

The notion followed is that of Grad where the product of two tensors is the sum of all possible permutations [22]. For example, $ua^{(2)} = u_i a_{jk} + u_j a_{ik} + u_k a_{ij}$ and u^3 is the direct vector product uuu. The fundamental thermohydrodyanmic variables ρ, u, θ, and P, the momentum flux tensor, can be expressed as linear combinations of the first three, up to second order, expansion coefficients. The heat flux, Q, is a linear combination of of the first four coefficients, $Q = a^{(3)} - ua^{(2)} - (D-1)\rho u^3$.

The mutual orthogonality of the Hermite polynomial basis ensures that the truncated series preserves the moments up to the order of truncation. This allows a fluid dynamics system to be construed by a finite set of macroscopic variables that are thermodynamic moments of the distribution functions. The moments, in turn, can be exactly found from the truncated series

$$f^N(x,\xi,t) \approx f^N(x,\xi,t) = \omega(\xi)\sum_{n=0}^{N}\frac{1}{n!}a^{(n)}(x,t)H^{(n)}(\xi) \tag{3.34}$$

3.1.6 Discrete Velocity Space

In this section, the Boltzmann-BGK equation is approximated by a finite Hermite expansion. It is important to note that the Hermite series can be completely and uniquely determined by the

values of the discrete abscissaes. This is due to the fact that the truncated distribution function can be represented as

$$f^N(x,\xi,t)H^{(n)} = w(\xi)p(x,\xi,t) \tag{3.35}$$

where p is a polynomial of degree $2N$ in ξ. The coefficients, $a^{(n)}$, can be expressed as an integral to be exactly evaluated by Gauss-Hermite quadrature.

$$a^{(n)}(x,t) = \int w(\xi)p(x,\xi,t)\ \mathrm{d}\xi = \sum_{a=1}^{d} w_\alpha p(x,\xi_\alpha,t) = \sum_{a=1}^{d} \frac{w_\alpha}{\omega(\xi_\alpha)} f^N(x,\xi_\alpha,t)H^N(\xi_\alpha) \tag{3.36}$$

where ξ_α are the discrete velocity and w_α are the abscissae of the Guass-Hermite quadrature that exactly reproduce the integral. Therefore, the conventional thermohydrodynamic variables can be replaced and the fluid system can be defined by a new set of fundamental variables $f^N(x,\xi_\alpha,t)$. That is, if f^N is known, then the first N the conventional thermohydrodynamic moments will be known.

The governing equations for $F^N(\xi_\alpha)$ are found by projecting the Boltzmann transport equation onto the Hermite basis and evaluating at the discrete velocity ξ_α. This is done term by term for the series representation Eq(3.33). The equilibrium distribution function given by the Maxwell-Boltzmann equation, Eq(3.27), is of the most interest. The coefficients, $a_{eq}^{(n)}$, are given by

$$a_{eq}^{(n)} = \int f_{eq}H^{(n)}(\xi)\ \mathrm{d}\xi \tag{3.37}$$

The Maxwell-Boltzmann distribution function can be represented as

$$f_{eg} = \frac{\rho}{\theta^{D/2}}\omega\left(\frac{\xi-u}{\sqrt{\theta}}\right) \tag{3.38}$$

where $\theta = T/T_0$ and the gas constant has been set to one. A change of variables $(\xi-u)/\sqrt{\theta} \to y$ leads to a simple integration

$$a_{eg}^{(n)} = \rho \int \omega(y) H^{(n)}(y\sqrt{\theta} + u)\ \mathrm{d}y \tag{3.39}$$

Carrying out the integration, the leading Hermite coefficients are found to be

$$\begin{aligned} a_{eq}^{(0)} &= \rho \\ a_{eq}^{(1)} &= \rho u \\ a_{eq}^{(2)} &= \rho(u^2 + (\theta - 1)\delta) \\ a_{eq}^{(3)} &= \rho(u^3 + (\theta - 1)\delta u) \\ a_{eq}^{(4)} &= \rho(u^2 + (\theta - 1)\delta u^2 + (\theta - 1)^2\delta^2) \end{aligned} \tag{3.40}$$

The particle and energy equilibrium distribution functions to second order in u, in the Hermite basis are

$$\begin{aligned} f_{eq}(x, \xi_\alpha, t) &= \omega(\xi_\alpha)\rho\left(1 + u_\alpha + \frac{u_\alpha^2 - u^2}{2} + (\theta - 1)\frac{\xi_\alpha^2 - D}{2}\right) \\ h_{eq}(x, \xi_\alpha, t) &= \omega(\xi_\alpha)p\left(1 + u_\alpha + u^2 + (\xi_\alpha^2 - D)\right) + E f_{eq} \end{aligned} \tag{3.41}$$

The weights, ω, have no temperature dependence, unlike the Taylor expansion derivation. This allows for variation of the temperature, instead of fixing the temperature to a reference temperature. The temperature is also present in the particle distribution function. The discrete algorithm is found by integrating spatially along the characteristic line.

$$f_\alpha(x + c\delta_t, t + \delta_t) - f_\alpha(x, t) = \int_0^{\delta_t} \Omega_f(x + ct', t + t')\mathrm{d}t' \tag{3.42}$$

where Ω_f is the BKG collision term. The above integral is evaluated using the trapezoidal rule, and the standard evolution equation is obtained. Via a similar procedure, the evolution equation of the internal energy is found.

$$\begin{aligned} f_\alpha(x+c\delta_t, t + \delta_t) - f_\alpha(x, t) &= -\frac{\delta_t}{\tau_f}[f_\alpha(x, t) - f_\alpha^{eq}(x, t)] \\ h_\alpha(x+c\delta_t, t + \delta_t) - h_\alpha(x, t) &= -\frac{\delta_t}{\tau_f}[h_\alpha(x, t) - h_\alpha^{eq}(x, t)] + (\frac{1}{\tau_f} - \frac{1}{\tau_h})Z_\alpha(f_\alpha(x, t) - f_\alpha^{eq}(x, t)) \end{aligned} \tag{3.43}$$

This above equation along with the equilibrium distribution functions, Eq(3.41), constitute the Hermite expansion thermal lattice Boltzmann method (TLB). To summarize, this method is most desirable as it allows for explicit coupling between the momentum and energy equation. Therefore, it accounts for how temperature affects velocity. This is the main improvement over the other methods presented.

3.1.7 Boundary Conditions

For any partial differential equation boundary conditions must be specified. We will focus on fluid flow in a pipe with wall at top and bottom of the domain and an inlet to the left and outlet to the right of the domain. At the walls, boundary conditions must be employed to determine the unknown components of the distribution function. Boundary condition can also be specified at the inlet, but we will not be concerned with those. Let us begin with the simpler case of the particle distribution function. At the boundary we ansatz that f is given by

$$f_\alpha = f_\alpha^* + \frac{\omega_\alpha}{c}\xi_\alpha \cdot Q \tag{3.44}$$

where f^* is a known local value and Q is a corrector term. Consider the top wall, moving with velocities (u, v). The unknown distribution function are f_7, f_4, and f_8. By writing out the equations for density and the macroscopic velocity, one can solve for the unknown functions.

$$\begin{aligned}
\rho &= f_0 + f_1 + f_2 + f_3 + (f_4^* - \omega_4 Q_y) + f_5 + f_6 + (f_7^* - \omega_7(Q_X + Q_y)) + (f_8^* + \omega_8(Q_x - Q_y)) \\
\rho u &= f_1 + f_5 + (f_8^* + \omega_8(Q_x - Q_y)) - f_3 + f_6 - (f_7^* - \omega_7(Q_x + Q_y)) \\
\rho v &= f_2 + f_3 + f_6 - (f_8^* + \omega_8(Q_x - Q_y)) - (f_4^* - \omega_4 Q_y) - (f_7^* - \omega_7(Q_x + Q_y))
\end{aligned} \tag{3.45}$$

There are several choices for $f*$.

(1) $f^*(x,t) = f(x, \xi_\alpha, t)$

(2) $f^*(x,t) = f(x, \xi_\alpha, t - \Delta t)$

(3) $f^*(x,t) = f_{eq}(x, \xi_\alpha, t)$

(4) $f^*(x,t) = 0$

The first option, (1), is the standard bounce back. The second, (2), is to use the distribution function from the previous time step, and the third, (3), is to use the equilibrium distribution function. All but the last scheme, (4), have been shown numerically to be valid. For this work the standard bounce back, the first option, is used. Once f^* is specified, and u and v on the boundary are known, the above system can be solved for the unknown distribution functions.

$$\begin{aligned} \rho &= \frac{1}{1+v}(f_0 + f_1 + f_3 + 2(f_2 + f_5 + f_6)) \\ f_4 &= f_2 - \frac{2}{3}\rho v \\ f_7 &= f_5 + \frac{1}{2}(f_1 - f_3) - \frac{1}{2}\rho u - \frac{1}{6}\rho v \\ f_8 &= f_6 - \frac{1}{2}(f_1 - f_3) + \frac{1}{2}\rho u - \frac{1}{6}\rho v \end{aligned} \tag{3.46}$$

A similar process can be done for the internal energy distribution function. The correction term, G_c, is proportional to the temperature difference. The relevant equations for a node at the north boundary are;

$$\begin{aligned} g_\alpha &= g^*_\alpha + \omega_\alpha G_c \\ \rho\epsilon^* &= g_0 + g_1 + g_2 + g_3 + g^*_4 + g_5 + g_6 + g^*_7 + g^*_8 \\ G_c &= \frac{\rho\epsilon - \rho\epsilon^*}{\omega_4 + \omega_7 + \omega_8} \end{aligned} \tag{3.47}$$

If the temperature is known on the boundary, then $\rho\epsilon$ can be easily calculated. For a detailed discussion see Liu, Lin and Mai 2009 [35] .

3.2 Numerical Test Problems

3.2.1 2D Thermal Poiseuille Flow

Here a fully developed flow in a channel is used to asses the accuracy of the various lattice Boltzmann methods. Both walls are held at a constant temperature T_0. The flow is driven by

an applied pressure gradient, see Fig(3.4). The flow is controlled by the Reynolds number is $Re = U_0 H/\nu$ in a channel of height H, where the maximum fluid velocity is U_0. The Prandtl number, $Pr = \nu/\chi$, controls the amount of viscous heat dissipation. The analytic solutions for the velocity and temperature profiles are

$$\begin{aligned} u(y) &= U_0\left(1 - y^2/H^2\right) \\ T(y) &= T_0 + \frac{1}{3} Pr U_o^2 \left[1 - \left(\frac{2y}{H} - 1\right)^4\right] \end{aligned} \tag{3.48}$$

The density is constant and set to unity. As the flow is fully developed, there is no x dependence in the solution. The velocity and temperature profiles are the same at all x locations. A 128×256 grid was used. Periodic boundary conditions were used in the $\hat{x}$ direction to simulate an infinite channel. The force from the pressure gradient was calculated and applied appropriately to all particles. The inlet and outlet pressures were not specified. As seen in Fig(3.5) and Fig(3.6), the simulated values are in excellent agreement with the analytic results.

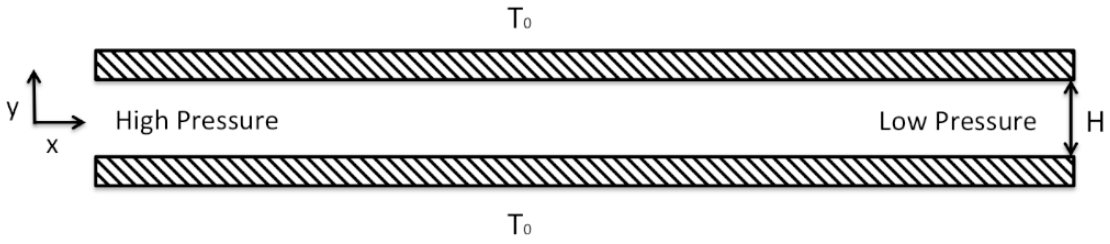

Figure 3.1: The schematic setup of Poiseuille flow. The flow is driven by a pressure gradient. Both the top and bottom walls are stationary and held at the same constant temperature. For Couette flow the pressure gradient is removed, the top and bottom wall are held a different temperatures, and the top wall move to the right with velocity u_t.

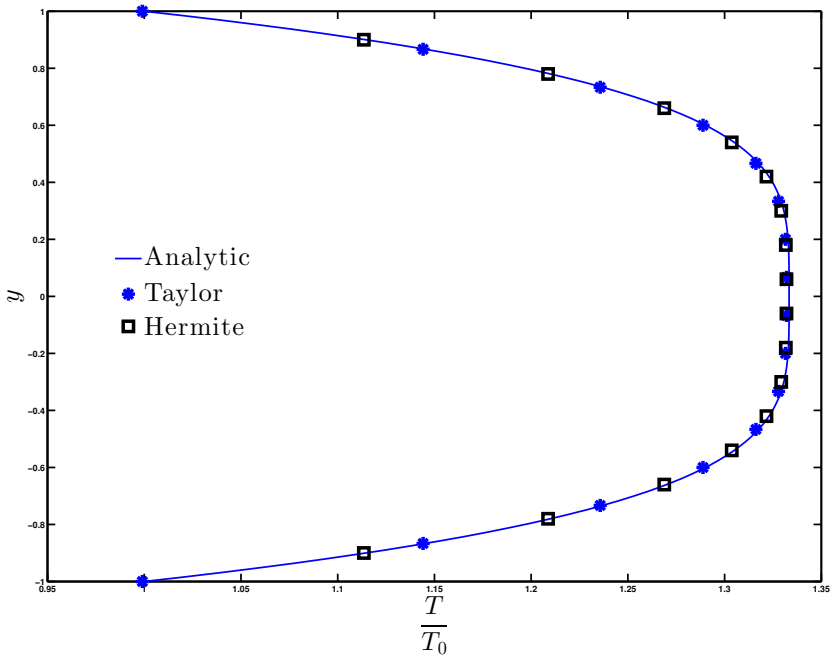

Figure 3.2: The temperature profile for a Poiseuille flow with $Pr = 1$. The solid line denotes the analytic solution, dots are the simulates values using the TLB and squares at the results of the HLB.

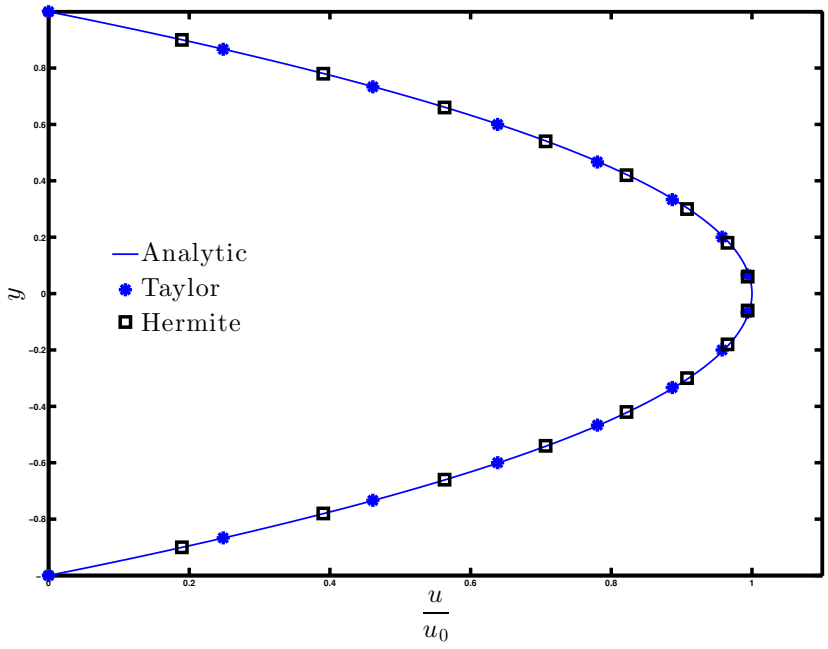

Figure 3.3: The velocity profile of a Poiseuille flow. The solid line denotes the analytic solution, dots are the simulates values using the TLB and squares at the results of the HLB.

3.2.2 2D Thermal Couette Flow

In this section, we verify that the boundary conditions work on a moving wall. The top wall moves at a constant velocity u_t. The top and bottom walls are held at constant temperatures T_t and T_b respectively. The momentum equation is

$$\frac{\partial}{\partial y}\left(\mu\frac{\partial u}{\partial y}\right) = 0 \tag{3.49}$$

where μ is the fluid viscosity. The energy equation is

$$\rho\left(u\frac{\partial h}{\partial x} + v\frac{\partial h}{\partial y}\right) = \frac{\partial}{\partial y}\left(k\frac{\partial T}{\partial y}\right) + \mu\left(\frac{\partial u}{\partial y}\right)^2 \tag{3.50}$$

where ρ, T, and h are the fluid density, temperature and enthalpy respectively. The thermal conductivity is given by k. This can be reformulated in terms of temperature

$$\rho c_p\left(u\frac{\partial T}{\partial x}+v\frac{\partial T}{\partial y}\right)=\frac{\partial}{\partial y}\left(k\frac{\partial T}{\partial y}\right)+\mu\left(\frac{\partial u}{\partial y}\right)^2 \tag{3.51}$$

where c_p is the specific heat. The energy equation, Eq(3.51), is valid for both ideal fluids and fluids with negligible compressibility effects. For a fully developed flow there is no variation in the $\hat{x}$ direction, leading to the simplification.

$$\frac{\partial}{\partial y}\left(k\frac{\partial T}{\partial y}\right)+\mu\left(\frac{\partial u}{\partial y}\right)^2=0 \tag{3.52}$$

The second term represents viscous dissipation.

The Reynolds number is $Re = u_t H/\nu$, in a channel of height H. The major control parameters are the Prandtl number and the Eckart number $Ec = u_t^2/(C_v\Delta T)$, where ΔT is the temperature difference between the channel walls. The Brinkman number $Br = PrEc$ controls the viscous heat dissipation. The analytic solution to the temperature profile is

$$T(y)=T_b+\frac{y\Delta T}{H}\left[1+\frac{Br}{2}\left(1-\frac{y}{h}\right)\right] \tag{3.53}$$

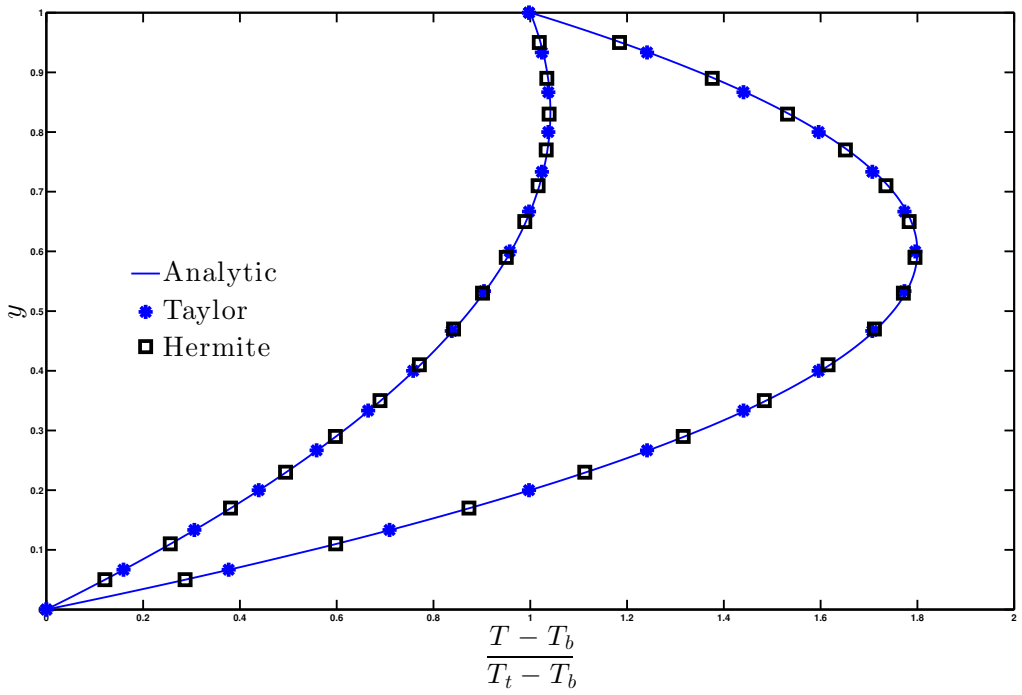

Figure 3.4: The temperature profile of a thermal Couette flow simulated on a 128×64 grid. The solid line denotes the analytic solution, dots are the simulates values using the TLB and squares at the results of the HLB.

Simulations were carried out to asses the relative error in both the velocity and temperature profiles across a range of parameters. The relative error is given by

$$E(\phi) = \frac{\sqrt{\sum_i |\phi_i - \phi_a(x_i)|^2}}{\sqrt{\sum_i |\phi_a(x_i)|^2}} \tag{3.54}$$

where ϕ_i are the measure value at grid point i and ϕ_a is the true analytic value. The code was run for 100,000 iterations on several sizes of grids. After convergence to the steady state, there were no appreciable deviations from the solution. Periodic boundary conditions were employed in the $\hat{x}$ direction to simulate an infinite channel. A bounce back plus correction term, as discussed in subsection 3.3.7, were implemented in the $\hat{y}$ direction. Analytic results agree well with the analytic results. The error was calculated on four lattice sizes and seen to decrease as second order in space. Given the success of the lattice Boltzmann simulations on the test problems we are ready to model

the elliptic flow observed in unitary fermi gases.

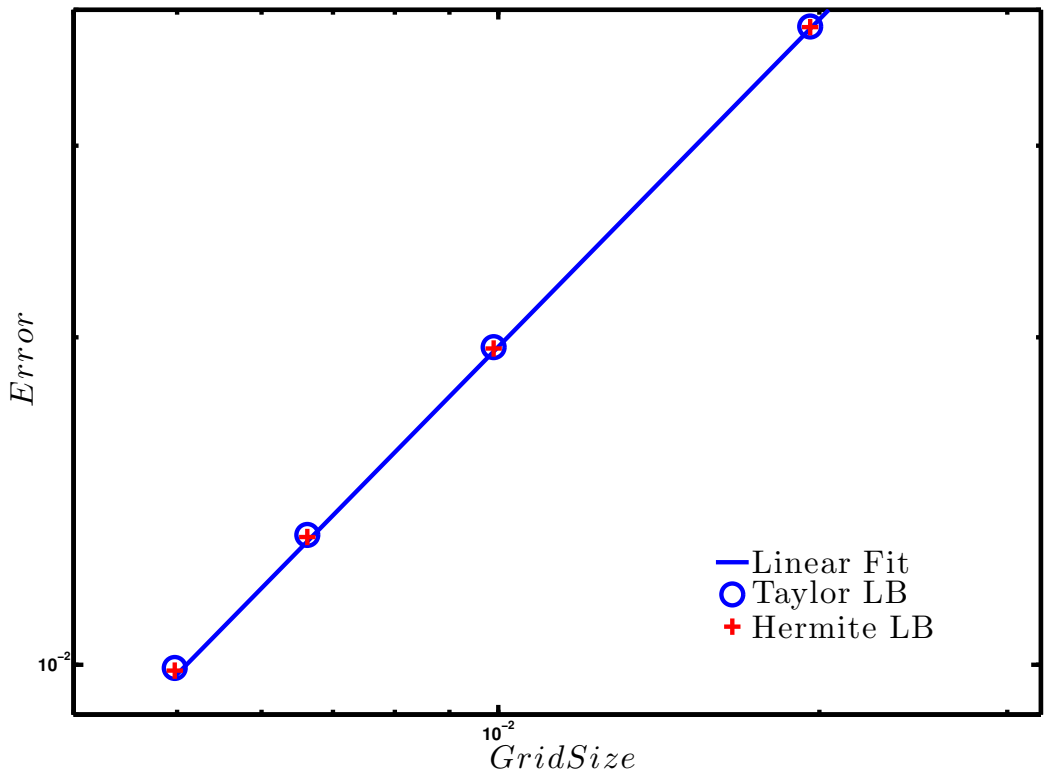

Figure 3.5: The relative error for a thermal Couette flow with $Br = 10$. The flow was simulated on square lattice with $N = 51, 101, 151, 201$ grid points using the HLB, crosses, and TLB, circles. The slope of the fitted line to the HLB is 1.96, confirming that the lattice Boltzmann simulations are of second order accuracy in space.

Chapter 4

Elliptic Flow

4.1 Introduction

The first physical demonstration of the nearly perfect fluidity of unitary fermi gases was the observation of elliptic flow by O'Hara [38]. In his experiment, a dilute unitary fermi gas was released from an elliptical, cylindrically symmetric trap. An anisotropic expansion occured, as can be seen in Fig(4.1). This anisotropic expansion is a signature of superfluidity and a sign of a strongly interacting system, as non-interacting systems expand isotropically. The density profiles at various times can be seen in Fig(3.2).

To measure the viscosity, hydrodynamic scaling solution are developed with one free fitting parameter related to the viscosity. This parameter is adjusted to minimize the standard χ^2 fit measure, as described in section 3.2. The results from Cao's study are in Fig(4.3) [12]. While this method yields an excellent agreement with the data, there are several unanswered questions. The topic we investigate in this chapter, is the simulation of elliptic flow with lattice Boltzmann methods.

Hydrodynamics is a valid when Knudsen number $Kn = l_{mfp}/R$, where l_{mfp} is the mean free path and R is the length scale of interest, is much less than unity. The characteristic length scale of our cold atom systems is the radial, or narrow width of the cloud. This give a Knudsen number of [13]

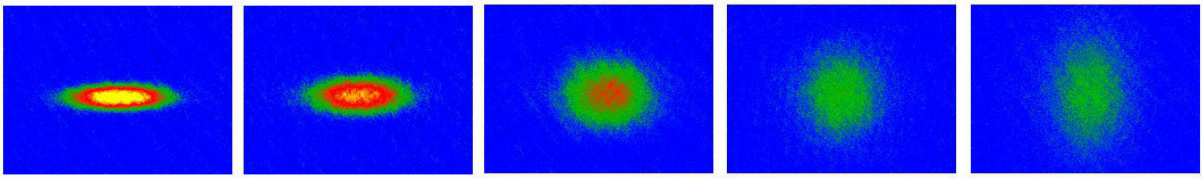

Figure 4.1: Cloud absorption images for expansion times $T = 0.2,\ 0.3,\ 0.6,\ 0.9,\ 1.2$ ms, $E = 2.3E_F$. Reproduced from [12]

$$Kn = \frac{3\pi^{3/2}}{(3N\lambda)^{1/3}}\left(\frac{T}{T_F}\right)^2 \tag{4.1}$$

where the aspect ratio is λ and N is the total number of particles. The aspect ratio is defined as $\lambda = \sigma_x/\sigma_z$, where σ_i is the standard deviation of Gaussian fit to the density profile. The initial aspect ratio is about $\lambda \approx 0.035$ and $N \approx 4 \times 10^5$. Therefore, hydrodynamic theory should work well for $T/T_F \leq 1.5$. As the cloud expands both the characteristic size and the mean free path change. However, as the expansion is much faster in the two traverse directions and there is effectively no expansion in the longitudinal direction, l_{mfp} decreases faster than R. Thus the Knudsen number decreases with time.

In the regime where the Knudsen number is not small, kinetic theory describes the dynamics. Common examples of this are microfluidic systems and rarefied gases. The Boltzmann transport equation Eq(3.1) is the governing equation of such systems. The remarkable fact of the Boltzmann equation is that it successfully reproduces the Navier-Stokes equation under the appropriate conditions. Lattice Boltzmann simulations are a popular technique for caring out fluid dynamics simulation. In this chapter we simulate the anisotropic expansion using lattice Boltzmann techniques.

This chapter is organized as follows. First, the relevant hydrodynamic equations are presented and scaling solutions are developed. Then simulation procedure are discussed. Last, simulation results are given and analyzed.

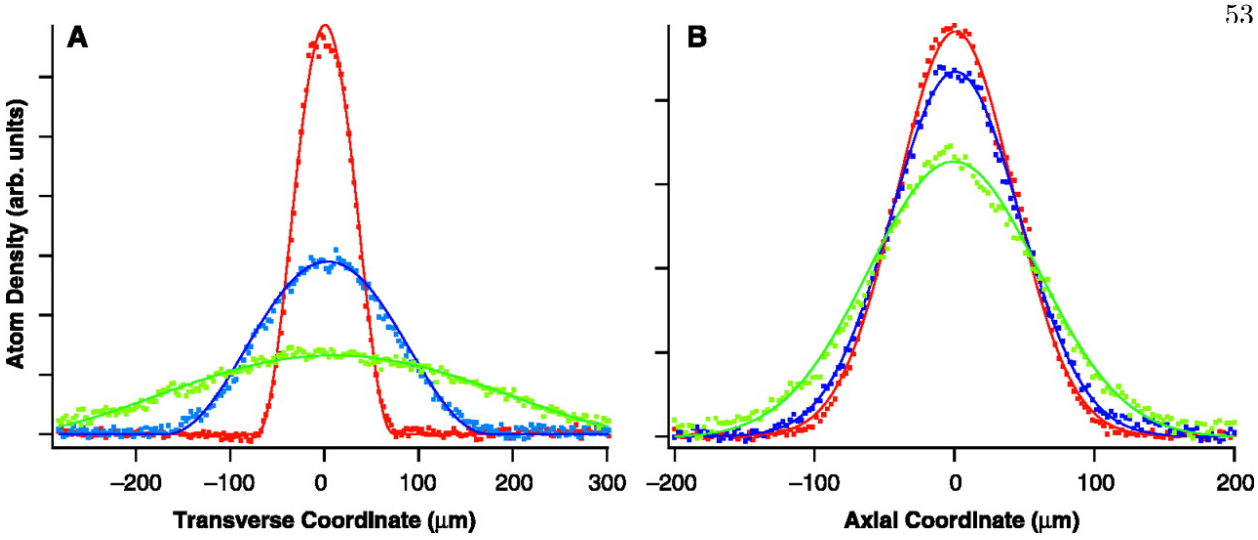

Figure 4.2: One-dimensional spatial distributions in the transverse (A) and axial (B) directions (red, 0.4 ms; blue, 1.0 ms; green, 2.0 ms). The data is fit with Gaussians from which the standard deviation defines the aspect ratio. Reproduced from [38]

Experimental procedures and results follow.

4.2 Hydrodynamics and Scaling Solution

The governing hydrodynamic equation for a single component fluid is

$$m(\partial_t + v \cdot \nabla)v_i = f_i + \sum_j \frac{\partial_j(\eta\sigma_{ij} + \zeta\sigma'_{ij})}{n} - \partial_i U_{trap} \tag{4.2}$$

where $f = -\nabla P/n$ is the force per particle from the pressure, m is the atomic mass, and U_{trap} is the trapping potential. The summation term accounts for viscous heating effects from the shear and bulk viscosities η and ζ, respectively, with $\sigma_{ij} = \partial v_i/\partial x_j + \partial v_j/\partial x_i - 2/3\delta_{ij}\nabla \cdot v$ and $\sigma'_{ij} = \delta_{ij}\nabla \cdot v$ In the unitarity limit Eq(4.2) can be simplified as $P = 2\mathcal{E}/3$. Exploiting this fact along with the energy equation one finds

$$m(\partial_t + v \cdot \nabla + 5\nabla \cdot v/3)P = 2\dot{q}/3 \tag{4.3}$$

where the frictional heating rate per volume is given by $\dot{q} = \sum_{ij} \sigma_{ij}^2/2 + \xi(\nabla \cdot v)^2$

The evolution equation governing the force per particle is easily found by differentiating Eq(4.3) with respect to x_i and using the continuity equation.

$$m(\partial_t + v\cdot\nabla + \frac{2}{3}\nabla\cdot v)f_i + \sum_j(\partial_i v_j)f_i - \frac{5}{3}(\partial_i\nabla\cdot v)\frac{P}{n} = -\frac{2}{3}\frac{\partial_i\dot{q}}{n} \tag{4.4}$$

The equation above governs the dynamics after the trapping potential is removed. The initial condition is set by the trapping potential, $f_i(t=0) = \partial_i U_{trap}$.

These equations are greatly simplified when the cloud is released from a deep harmonic potential. Under such conditions, the force, f_i, is linear in the spacial coordinates. Then, in the zero viscosity limit the force remains linear as the cloud expands and evolves. Thus, the velocity is linear in the spacial coordinate. With a linear velocity profile, the pressure term, $\frac{5}{3}(\partial_i\nabla\cdot v)\frac{P}{n}$, vanishes. For small viscosities, numerical integration has shown viscous dissipation works to restore a linear flow field, with minimal non-linearity [45]. Therefore in the unitary limit, the evolution of Eq(4.4) is only weakly dependent on the precise spacial profile of the pressure, and independent of other thermodynamic properties.

4.2.1 Scaling Solutions

For the development of our scaling solution we assume that the velocity is precisely linear in the coordinates. The force shall be taken as $f_i(t,x) = a_i(t)x_i$. In the high temperature limit, the density profile is Gaussian. We will use $n = n_0\exp[-\sum_i x_i/b_i(t)]$. The central density, n_0, is determined from the total number of particles, N, to be, $n_0 = N/(\pi^{3/2}b_x b_y b_z)$. The velocity field is found using current conservation and requiring that the pressure vanish, $v_i = x_i\dot{b_i}/b_i$.

The bulk viscosity is taken to be zero. For unitary fermi gasses this is believed to be an excellent approximation [13]. Universality dictates the shear viscosity's the dependence to temperature and density [45]. We pick a universal form of

$$\eta = \alpha(T/T_F)\hbar n \tag{4.5}$$

where the local fermi temperature is $T_F = \hbar^2(3\pi^2 n)^{2/3}/(2mk_b)$. In practice, $\alpha(T/T_F)$ is taken to be a constant. In the low density regions of the cloud $\eta \to 0$, as mandated by kinetic theory and required for energy conservation.

Given these assumption, the governing equation for our scaling parameters using Eq(4.4) yields

$$nx_i\left(\dot{a_i} + 2\frac{\dot{b_i}}{b_i}a_i + \frac{2}{3}\sum_j \frac{\dot{b_j}}{b_j}a_i\right) = -\frac{2}{3}\partial_i \dot{q} \tag{4.6}$$

Here the bulk viscosity has been set to zero. Multiplying by x_i and integrating over all space, the LHS gives $\int \mathrm{d}^2x n x_i^2 = N\langle x_i^2\rangle = N\langle x_i^2\rangle_0 b_i^2(t)$. The initial mean square size of the cloud, in the ith direction is $\langle x_i^2\rangle_0$. Assuming that $\eta \to 0$ sufficiently fast as the density approaches zero we find

$$\left(\dot{a_i} + 2\frac{\dot{b_i}}{b_i}a_i + \frac{2}{3}\sum_j \frac{\dot{b_j}}{b_j}a_i\right) = \frac{1}{3}\frac{\int \mathrm{d}^3x\ \eta}{N\langle x_i^2\rangle_0 b_i^2(t)}\sum_{ij}\sigma_{ij}^2 \tag{4.7}$$

Repeating the process for Eq(4.3) we find

$$\frac{\ddot{b_i}}{b_i} = \frac{a_i}{m} - \omega_i - \frac{\int \mathrm{d}^3x\ \eta}{mN\langle x_i^2\rangle_0 b_i^2(t)}\ \sigma_{ii} \tag{4.8}$$

The ω_i^2 term is set to zero as it arises from the trapping potential.

The trap averaged viscosity parameter can now be defined as

$$\bar{\alpha} \equiv \frac{1}{\hbar N}\int \mathrm{d}^3x \eta(x,t) \tag{4.9}$$

The trap averaged viscosity is determined by fitting the scaling solution to the experimental data. The aspect ratio, $\sigma_x(t)/\sigma_z(t) = \sqrt{\langle x^2\rangle/\langle z^2\rangle}$, can be observed experimentally as a function of time. The ODE's defining the scaling solution, Eq(4.7) and Eq(4.8), are solved numerically with the initial conditions of $\dot{b_i}(0) = 0$ and $a_i(0) = m\omega_i^2$, where ω_i is the trapping frequancy in the i^{th} direction. The aspect ratio, $\sigma_x(t)/\sigma_z(t) = (\omega_z/\omega_x)b_x(t)/b_z(t)$, is fit to the data by adjusting the one free parameter, $\bar{\alpha}$. See Fig(4.3).

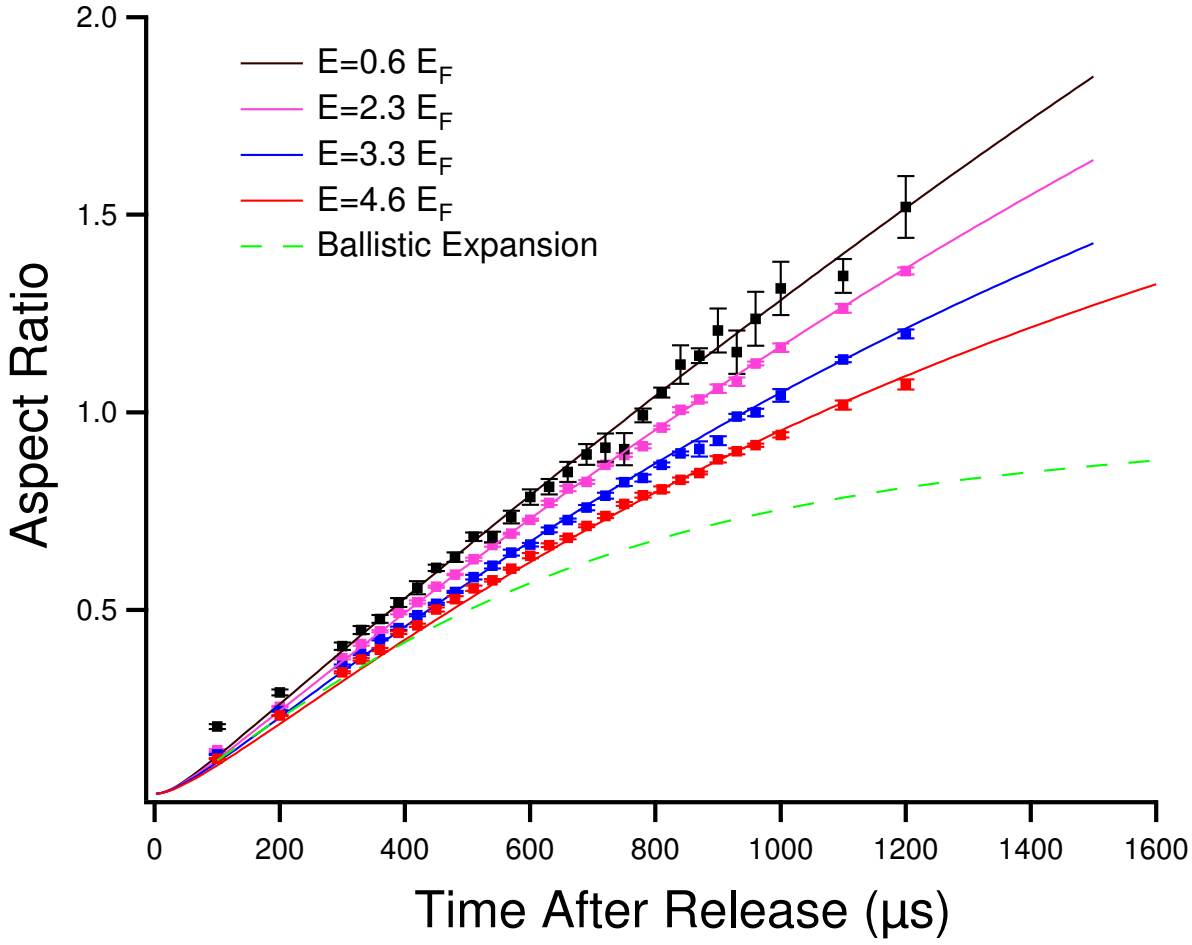

Figure 4.3: Aspect ratio versus time. The solid curves are the fitted scaling solutions, Eq(4.7) and Eq(4.8). The ballistic expansion is that of a non collisional gas, where the mean free path is greater that the system size. Error bars denote statistical fluctuations in the aspect ratio. Reproduced from [12]

4.3 Cold Atom Simulations

4.3.1 Boundary Effects

For the simulation of our cold atom systems we used periodic boundary conditions. The density is expected to decay exponentially. Therefore, if we simulate a sufficiently large physical space the edges to the lattice will contain effectively no mass. Periodic boundary condition will not effect the dynamics as there is effectively no forces exerted on the flow from the edges. To test this assumption and determine the appropriate lattice size needed, we simulated at the same initial condition and resolution on several different lattice sizes. When lattice of different size have the same behavior, edge effect are negligible. This will correspond to a decay of the density to zero at the edge of the lattice. See Fig(4.5) and Fig(4.6).

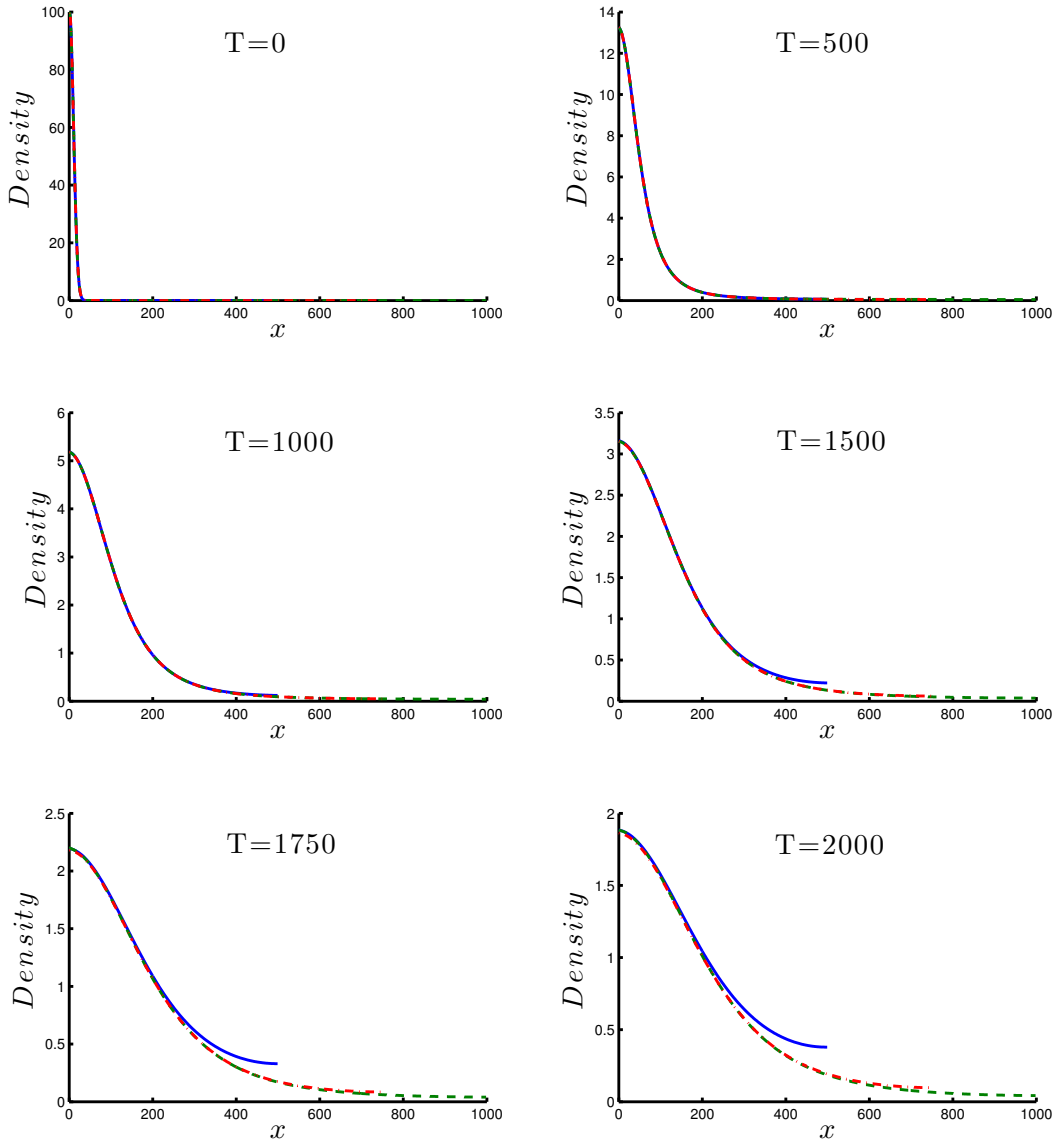

Figure 4.4: The x density profile, in lattice units, on three sizes of lattice at various lattice times, in lattice units: 1000×1500 blue, 1500×2250 green dashed, 2000×3000 red dashed. The effect of the periodic boundary conditions can be seen on the small (blue) lattice as it does not decay to zero. The two large lattices have equivalent behavior. Thus, edge effects are negligible. The finite size effects are less in the y direction.

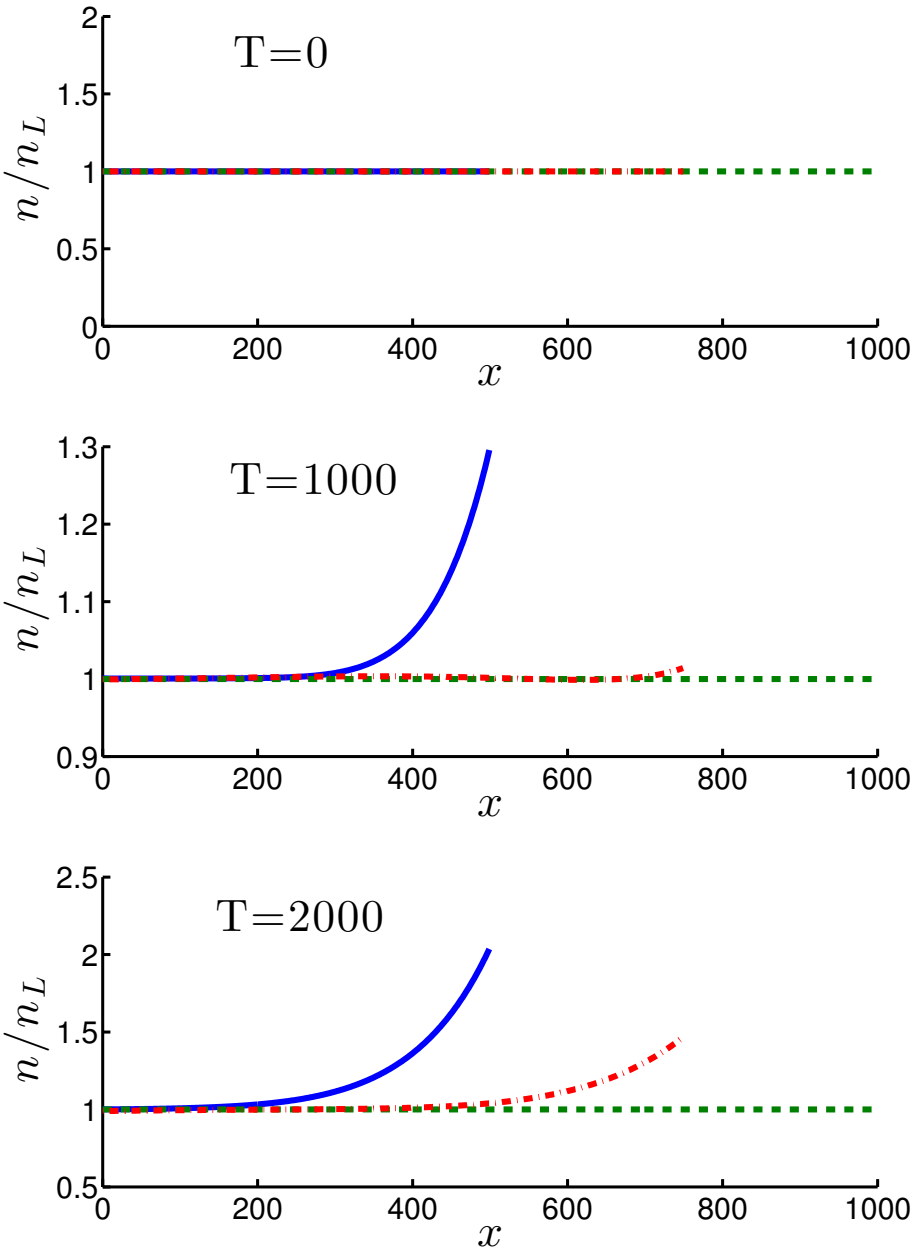

Figure 4.5: The x density profile normalized by the density profile from the largest lattice, in lattice units, at various times. The lattice sizes are 1000×1500 blue, 1500×2250 green dashed, 2000×3000 red dashed. The boundary effects can be seen by looking at precent difference between the varying lattice sizes. While the precent difference between the largest two lattices is appreciable the actual difference is small as seen in the previous figure.

4.3.2 Convergence of Solution

Lattice Boltzmann is a second order method, meaning that the error in the simulation decreases quadratically as the spacial resolution increases, Error $\sim (\Delta x)^2$. In order to resolve the exponential decrease in density a very fine resolution was used. To determine this resolution, several grid resolutions were run until they converged to a stable solution.

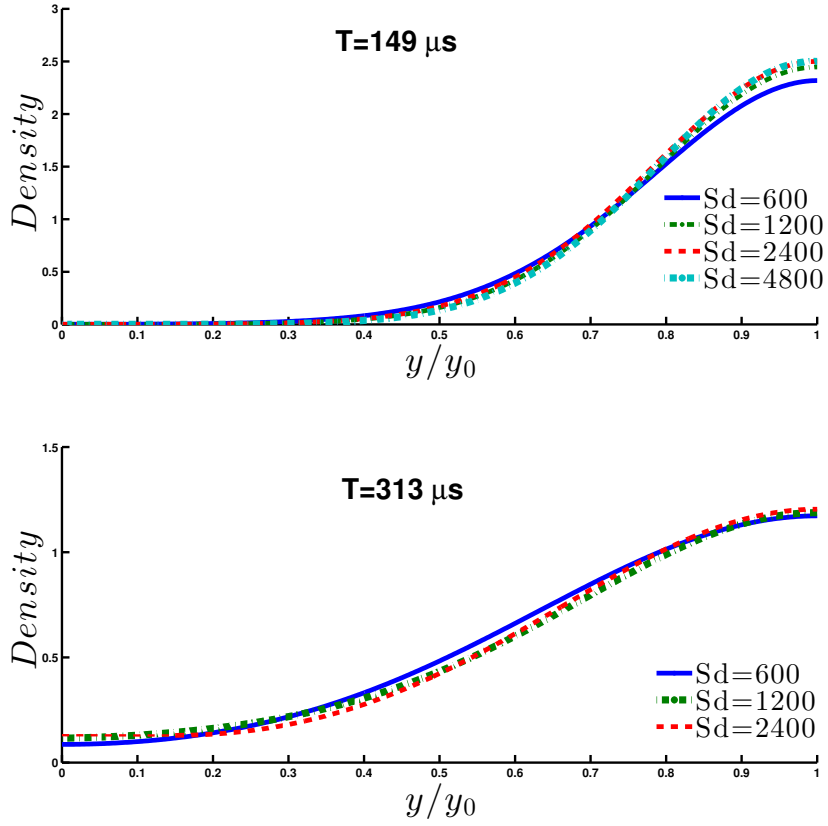

Figure 4.6: The y density profile at different resolutions at various times. The resolution can be measured by the standard deviation, *sd*, of the initial Gaussian in lattice units. The larger the standard deviation, the finer the resolution. The red and green lines are very close indicating convergence of solutions. Despite the difference in the profile of about 2%, the measured aspect ratios differ by 0.76%.

A spacial resolution of $\Delta x = 0.1\mu$m was used for the simulation. The difference of about 2% in the narrow density profile was observed between the lattice resolutions of $\Delta x = 0.1\mu$m and $\Delta x = 0.025\mu$m. This corresponded to a difference in the aspect ratio of about one precent. Therefore, we expect the error due to the spacial resolution to be about one percent.

4.4 Results

4.4.1 Isothermal Lattice Boltzmann

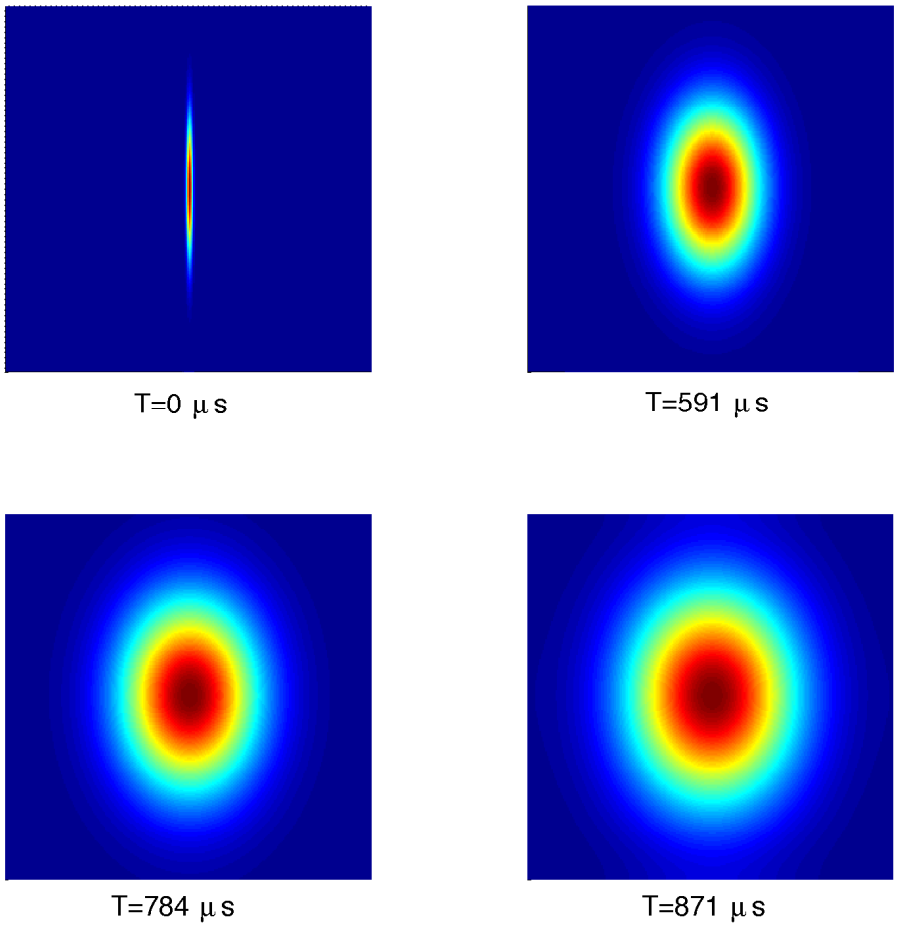

Figure 4.7: The density surfaces of the expansion at various times for τ =constant model.

We investigated two relaxation time models. The first models investigated incorporated a constant relaxation time. The second model employed was based off the scaling solutions. The relaxation time was set to $\eta = \bar{\alpha} n$. The second model is an approximation of based on Braby's result that the density should be proportional to $\eta \propto (mT)^{3/2}$ [8]. As this is an isothermal lattice Boltzmann, the thermodynamic result that $mT \propto n^{2/3}$, gives the form assumed before of $\eta = \bar{\alpha} n$ [45]. The fitting parameter, $\bar{\alpha}$, values were take from Cao's thesis [13]. For our simulation of the a unitary fermi gas with $E = 4.6 E_F$ the correspond value of the fitting parameter is $\bar{\alpha} = 42.0$.

The result can be seen in Fig(4.8). Initially, there is excellent agreement between the simulation with $\eta = \bar{\alpha} n$. The deviation at later times could signal the transition to a three dimensional system. We plan to investigate this further using using 3D simulations. Interestingly, the density profile remains Gaussian, similar to Fig(4.9). The aspect ratio grows slowly after the deviation from the scaling solution and asymptotes to a value of about unity.

The result of the simulation with fixed relation time are surprising. Mainly, the slow nearly linear growth observed after the departure from the scaling solutions was unexpected. In the $\eta = \bar{\alpha} n$ model, the low density outer edge of the cloud is essentially free streaming, while when $\tau =$constant, collision are more prevalent. The difference in the prevalence of collision may account for the differing values where each model begins to deviate from the scaling solution. If the departure is indicative of the transition from a 2D to 3D, system the relaxation time model used will be important. In the 2D regime $\tau \sim V^{1/2}$, this becomes $\tau \sim V^{1/3}$ for the 3D regime. A density dependent relaxation time will do better accounting for this scaling change as the density is linked to the volume.

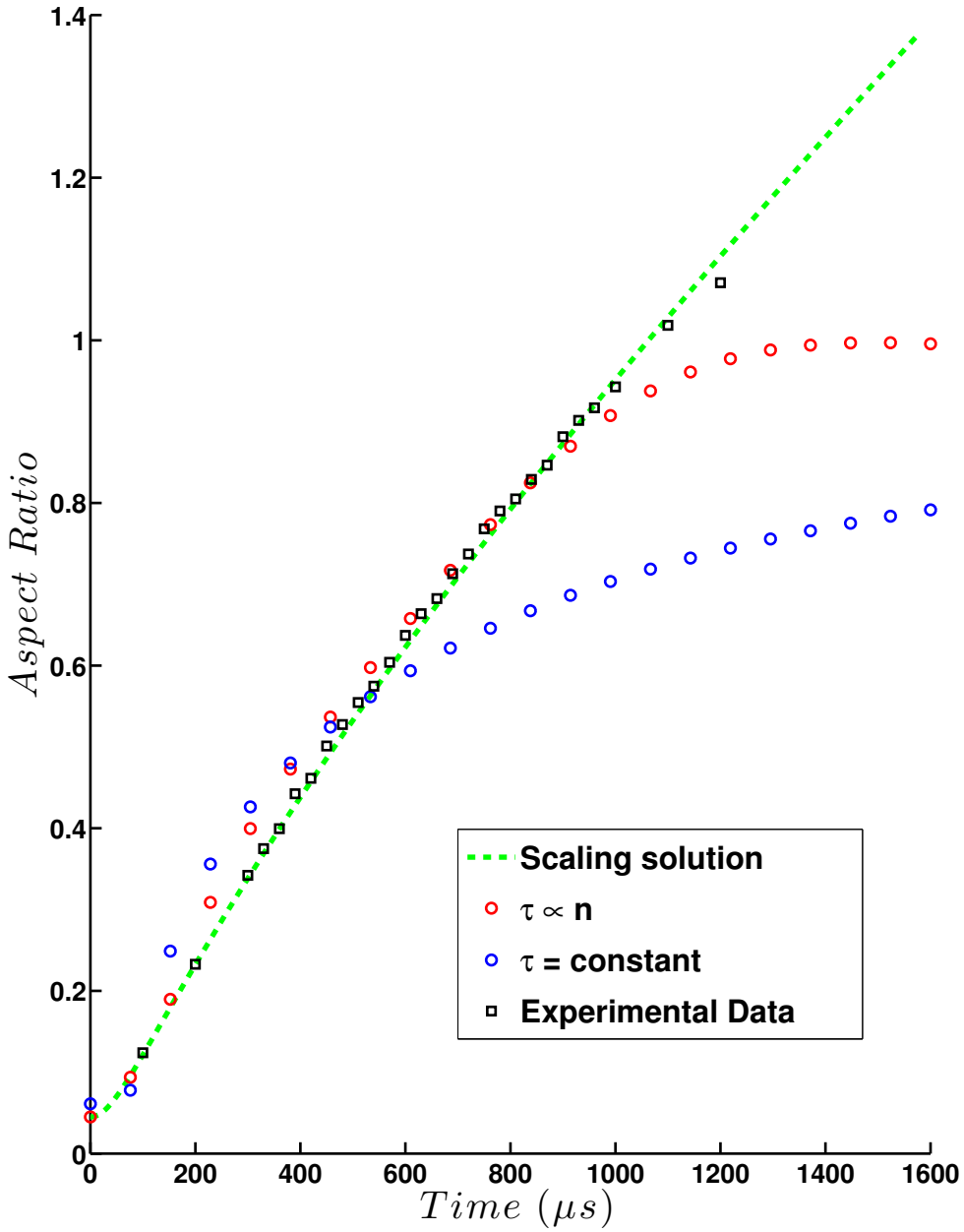

Figure 4.8: The aspect ratio versus expansion time. The black squares are the experimental data provided by Cao for a unitary fermi gas with $E = 4.6E_F$. The uncertainty is roughly the symbol size. The green line is the scale solution. The red dots are the simulation with $\eta = \bar{\alpha}n$. Agreement with the scaling solution is excellent until about 1000 μs. This could be the transition to a 3D system. The constant relaxation time, blue dots, show poor agreement with the experimental data.

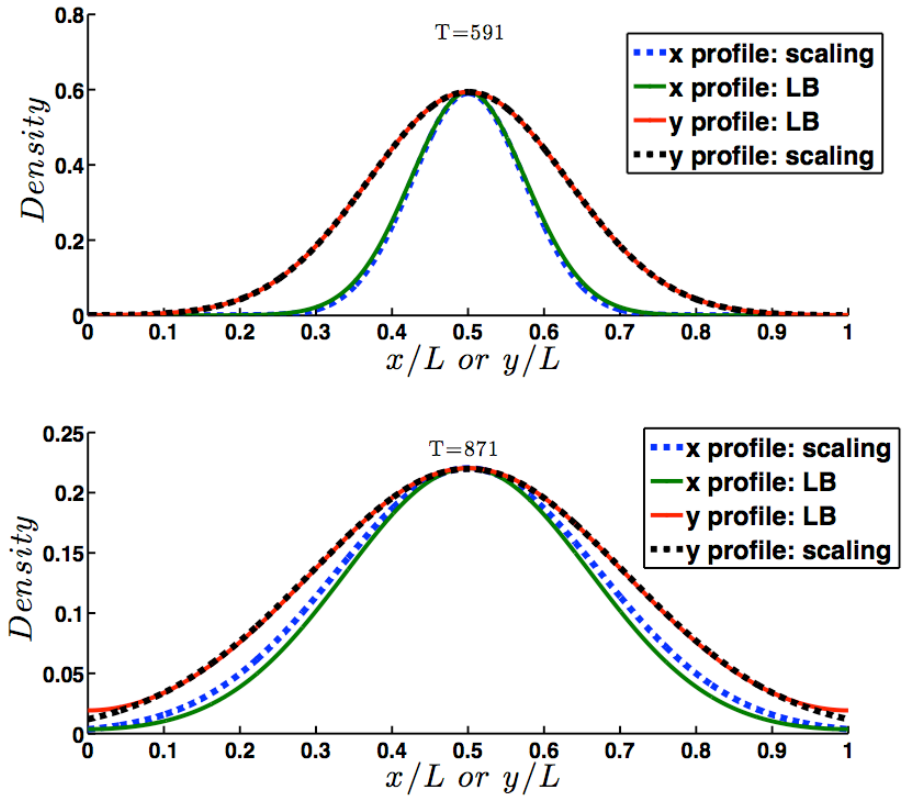

Figure 4.9: The density profiles, in lattice units, of the lattice Boltzmann simulation with τ =constant and the scaling solution at two different times. At $T = 591$ μs there is excellent agreement. At the later time the LB profile is still Gaussian but has deviated from the scaling solution. This is characteristic of the regime with slow linear growth of the aspect ratio. Very similar qualitative behavior was found for the density dependent relaxation time model, $\eta = \bar{\alpha}n$.

The asymptotic growth rates of the scaling can be found at early and late times [46]. These are first order hydrodynamic, or the Eulerian, growth rates. In the non-dimensional coordinate system

$$b_\perp = \begin{cases} 1 + \frac{1}{2}\omega_\perp t^2 + O(t^4) & \omega_\perp t \ll 1 \\ \frac{\omega_\perp t}{\sqrt{2/3}} + c_0 + O(t^{-1/3}) & \omega_\perp t \gg 1 \end{cases} \tag{4.10}$$

where $c_0 \approx 1.3$ is a numerically determined constant chosen to match the early and late time behaviors. The longitudinal expansion behavior is given by

$$b_L = \begin{cases} 1 + \frac{(\lambda\omega_\perp t)^2}{2} + O(t^4) & \omega_\perp t \ll 1 \\ a_0\lambda^2\omega_\perp t & \omega_\perp t \gg 1 \end{cases} \tag{4.11}$$

where a_0 is a constant. The crossing time, t_{cross}, happens when the longitudinal and transverse radius cross. At this time the aspect ratio is one. This happens at time

$$t_{cross} = \frac{\sqrt{2/3}}{\omega_x}(1 + O(\lambda)) \tag{4.12}$$

Note that the crossing time is solely dependent on the trap parameters, and that it is independent of the number of particles and thermodynamic variables such as initial energy. This gives a physical time of $t_{cross} = 816\mu$s. This is not in good agreement with our simulation or the experimental data. This is expected as dissipative effects are not accounted for.

The growth of the longitudinal direction is very slow. Therefore, the volume $V \sim t^2$. Once the longitudinal direction begins to grow, at time $t_{3d} \sim (\lambda^2\omega_\perp)^{-1} \geq 2000$ μs, the volume scales as $V \sim t^3$. This happens after t_{cross}. At these late times, our simulations are inconsistent with experimental data. We conclude that even though the growth in the longitudinal direction is after the time where our simulation deviate from the scaling solution, 3D effect are important at earlier times. As mentioned previously, the 3D volume will effect the relaxation time and therefore affect the evolution. We plan to investigate this further with $3D$ simulations.

4.4.2 Thermal Lattice Boltzmann

Let us first consider the Hermite projection lattice Boltzmann method, Eq(3.43). It was found to be very numerically unstable. Very quickly, on the order of tens of iterations, noise developed and the system failed. The location of the noise is dependent on the reference temperature, T_0 chosen. If the reference temperature was chosen so that the outer low density regions have reduced temperature, $\theta = T/T_0$, on the order of one, the noise first manifests in the inner high density region. Likewise, if the reference temperature was set so that $\theta \approx 1$ in the inner high density region, the noise develops in the outer low density region.

We suspect that instability is introduced in the equilibrium particle distribution function

$$f_{eq}(x,\xi_\alpha,t) = \omega(\xi_\alpha)\rho\left(1 + u_\alpha + \frac{u_\alpha^2 - u^2}{2} + (\theta-1)\frac{\xi_\alpha^2 - D}{2}\right) \tag{4.13}$$

The temperature term, $(\theta - 1)$, may differ from the velocity terms by several orders of magnitude. This leads to a noise growth in these regions and the ultimate failure of the simulation.

The Hermite projection lattice Boltzmann was where our computer time was spent. Very low resolution runs of the Taylor expansion method appeared not to suffer from the same numerical instabilities as the Hermite method. The density profile results are identical to those of the ILB. The temperature profile found will provide a starting point for comparison to coupled thermal lattice Boltzmann methods. The relaxation time of the internal energy distribution function is related to the thermal conductivity $\chi = (D+2)\tau_c RT/D$. The form of the thermal conductivity used was from Barby's work

$$\chi = \frac{225\alpha_t}{128\sqrt{\pi}} m^{1/2}\theta^{3/2} \tag{4.14}$$

where α_t is introduced as a free fitting parameter [8]. Further study is needed to investigate these models and their place for simulating unitary fermi gases, as there are large temperature variations.

Chapter 5

Summary and Outlook

Unitary fermi gases are a unique state of matter. Thanks to the control of the relevant system parameters, these gases provide a versatile tabletop system for studying many open problems in many body physics. The system is characterized by the lack of any intrinsic length scale, making it universal. That is, the transport coefficients and thermodynamic properties are independent of the interaction details. This introduces a difficultly, as there is no small parameter for perturbative studies. The strong interaction between atoms lead to an almost ideal hydrodynamic behavior. Therefore, unitary fermi gas systems are a candidate for prefect fluids, and as such the the ratio of shear viscosity to entropy, η/s, is of great interest. This interest is largely inspired by the string theory conjecture of a lower bound, $\eta/s \geq \hbar/(4\pi k_b)$, for a broad class of strongly interacting systems.

This dissertation reports on two topics pertinent to the hydrodynamic description of unitary fermi gasses. A stochastic formulation of hydrodynamics was developed. The stochastic formulation is intuitively pleasing as is contains the fluctuations present in statistical mechanics. This was done assuming small thermal fluctuations and a nearly linear response to them. The retarded correlation function between two stress tensors was calculated within this framework. The Kubo formalism of transport coefficients was then used to calculate a lower bound on viscosity. A function was fit to experimental thermodynamic data and used to evaluate the bound. This bound is consistent with the experimental measurements of viscosity. Therefore, the dissipation of momentum due to fluctuations appears to be a key feature in the discussion of perfect fluids.

The second part of the dissertation investigated elliptic flow of fermi gasses. This anisotropic flow is an indication of strongly interacting systems. Different lattice Boltzmann methods were employed to simulate elliptic flow. The standard isothermal lattice Boltzmann was used with two different viscosity models. A constant viscosity did not yield good agreement with the experimental data, although the density profiles remained Gaussian. The more realistic viscosity model, where viscosity is proportional to density, initially had good agreement with the experimental results. At later times a deviation occurred when the aspect ratio asymptotes to about one. This could signal the switch from an effectively 2D to 3D system. The density profile remained Gaussian. The Hermite expansion based thermal lattice Boltzmann was found to be numerically unstable, most likely due to the large temperature differences. The Taylor expansion based lattice Boltzmann method, which is limit to Boussinesq flow, shows promise and we plan to investigate this further.

There are many open questions regrading stochastic hydrodynamics and transport coefficients. The topic that we find most interesting are non-linear effect. Our formulation assumes a linear response and that the fluctuations are independent of the hydrodynamic variables. Intuitively, one expects the fluctuations to be dependent on both the local density and the temperature. This is known as multiplicative noise. Much progress has been made on simple generic systems, such as $dq/dt = -F(q) + e(q)\xi$, where ξ is a Gaussian white noise whose local amplitude is controlled by $e(q)$ [4] [5]. Currently, little progress has been made accounting for multiplicative noise within the hydrodynamic regime.

Using our lattice Boltzmann code there are several question we plan to investigate. It would be useful to compare the 2D and 3D simulations. At early times, the system is essentially two dimensional where $\tau \sim V^{1/2}$, and becomes more three dimensional as time increases, $\tau \sim V^{1/3}$. Freezeout is when a degree of freedom is no longer relevant. For a unitary fermi gas system the mean free path, l_{mfp}, and could size, R, are considered. In the cold atom systems, the behavior will change from hydrodynamic to ballistic, where no collision occur characterized by $l_{mph} \geq R$. This would be of interest to simulate. In addition, the effects of different models of thermal conductivity and the values of the pertinent constants can be studied with thermal lattice Boltzmann simulations

and compared to theoretical and experimental findings.

Acknowledgements

Chapter Two closely follows Professor Paul Romatschke's and my paper [42]. Figure(2.2,2.3) and much of the text is reproduced or paraphrased.

Bibliography

[1] Allan Adams, Lincoln D. Carr, Thomas Schfer, Peter Steinberg, and John E. Thomas. Strongly correlated quantum fluids: ultracold quantum gases, quantum chromodynamic plasmas and holographic duality. New Journal of Physics, 14(11):115009, November 2012.

[2] Allan Adams, Lincoln D. Carr, Thomas Schfer, Peter Steinberg, and John E. Thomas. Strongly correlated quantum fluids: ultracold quantum gases, quantum chromodynamic plasmas and holographic duality. New Journal of Physics, 14(11):115009, 2012.

[3] Mike H. Anderson, Jason R. Ensher, Michael R. Matthews, Carl E. Wieman, and Eric A. Cornell. Observation of bose-einstein condensation in a dilute atomic vapor. science, 269(5221):198–201, 1995.

[4] Peter Arnold. Langevin equations with multiplicative noise: Resolution of time discretization ambiguities for equilibrium systems. Phys. Rev. E, 61:6091–6098, Jun 2000.

[5] Peter Arnold. Symmetric path integrals for stochastic equations with multiplicative noise. Phys. Rev. E, 61:6099–6102, Jun 2000.

[6] R. Baier, P. Romatschke, D. T. Son, A. O. Starinets, and M. A. Stephanov. Relativistic viscous hydrodynamics, conformal invariance, and holography. arXiv e-print 0712.2451, December 2007. JHEP0804:100,2008.

[7] Jean-Paul Blaizot and Edmond Iancu. The quarkgluon plasma: collective dynamics and hard thermal loops. Physics Reports, 359(5):355528, 2002.

[8] Matt Braby, Jingyi Chao, and Thomas Schfer. Thermal conductivity and sound attenuation in dilute atomic fermi gases. Physical Review A, 82(3):033619, 2010.

[9] C. C. Bradley, C. A. Sackett, J. J. Tollett, and R. G. Hulet. Evidence of bose-einstein condensation in an atomic gas with attractive interactions. Physical Review Letters, 75(9):1687–1690, 1995.

[10] Stephen G. Brush. The kind of motion we call heat, volume 2. North-Holland Amsterdam, 1976.

[11] Georg Morten Bruun and Henrik Smith. Shear viscosity and damping for a fermi gas in the unitarity limit. Physical Review A, 75(4):043612, 2007.

[12] C. Cao, E. Elliott, H. Wu, and J. E. Thomas. Searching for perfect fluids: Quantum viscosity in a universal fermi gas. (1105.2496), May 2011. New Journal of Physics 13 (2011) 075007.

[13] Chenglin Caot. Universal Quantum Viscosity in a Unitary Fermi Gas. PhD thesis, Duke University, May 2012.

[14] Clifford Chafin and Thomas Schfer. Hydrodynamic fluctuations and the minimum shear viscosity of the dilute fermi gas at unitarity. Physical Review A, 87(2):023629, 2013.

[15] Laszlo P. Csernai, Joseph I. Kapusta, and Larry D. McLerran. Strongly interacting low-viscosity matter created in relativistic nuclear collisions. Physical review letters, 97(15):152303, 2006.

[16] K. B. Davis, M.-O. Mewes, MR van Andrews, N. J. Van Druten, D. S. Durfee, D. M. Kurn, and W. Ketterle. Bose-einstein condensation in a gas of sodium atoms. Physical Review Letters, 75(22):3969–3973, 1995.

[17] Brian DeMarco and D. S. Jin. Onset of fermi degeneracy in a trapped atomic gas. Science, 285(5434):1703–1706, 1999.

[18] Annunziata D'Orazio and Sauro Succi. Simulating two-dimensional thermal channel flows by means of a lattice boltzmann method with new boundary conditions. Future Generation Computer Systems, 20(6):935–944, 2004.

[19] Michael G. Endres, David B. Kaplan, Jong-Wan Lee, and Amy N. Nicholson. Lattice Monte Carlo calculations for unitary fermions in a finite box. Phys.Rev., A87:023615, 2013.

[20] Tilman Enss, Rudolf Haussmann, and Wilhelm Zwerger. Viscosity and scale invariance in the unitary fermi gas. Annals of Physics, 326(3):770796, 2011.

[21] Miguel Angel Escobedo, Massimo Mannarelli, and Cristina Manuel. Bulk viscosities for cold fermi superfluids close to the unitary limit. Physical Review A, 79(6):063623, 2009.

[22] Harold Grad. On the kinetic theory of rarefied gases. Communications on pure and applied mathematics, 2(4):331–407, 1949.

[23] Zhaoli Guo". Thermal lattice boltzmann equation for low mach number flows: Decoupling model. Physical Review E, 75(3), 2007.

[24] Zhaoli Guo, Chuguang Zheng, Baochang Shi, and T. S. Zhao. Thermal lattice boltzmann equation for low mach number flows: Decoupling model. Phys. Rev. E, 75:036704, Mar 2007.

[25] Xiaoyi He, Shiyi Chen, and Gary D. Doolen. A novel thermal model for the lattice boltzmann method in incompressible limit. Journal of Computational Physics, 146(1):282 – 300, 1998.

[26] Tin-Lun Ho. Universal thermodynamics of degenerate quantum gases in the unitarity limit. Phys. Rev. Lett., 92:090402, Mar 2004.

[27] Tin-Lun Ho. Universal thermodynamics of degenerate quantum gases in the unitarity limit. Physical review letters, 92(9):090402, 2004.

[28] Li-Hsin Hung and Jaw-Yen Yang. A coupled lattice boltzmann model for thermal flows. IMA Journal of Applied Mathematics, 76(5):774–789, 2011.

[29] K. Kovtun, P. D. T. Son, and A. O. Starinets. Viscosity in strongly interacting quantum field theories from black hole physics. Phys. Rev. Lett., 94:111601, Mar 2005.

[30] Pavel Kovtun. Lectures on hydrodynamic fluctuations in relativistic theories. arXiv e-print 1205.5040, May 2012. J. Phys. A: Math. Theor. 45 (2012) 473001.

[31] Pavel Kovtun, Guy D. Moore, and Paul Romatschke. Stickiness of sound: An absolute lower limit on viscosity and the breakdown of second-order relativistic hydrodynamics. Physical Review D, 84(2):025006, 2011.

[32] Mark JH Ku, Ariel T. Sommer, Lawrence W. Cheuk, and Martin W. Zwierlein. Revealing the superfluid lambda transition in the universal thermodynamics of a unitary fermi gas. Science, 335(6068):563567, 2012.

[33] L. D. Landau and E. M. Lifshitz. Fluid mechanics, vol. 6. Course of Theoretical Physics, page 227229, 1987.

[34] Q. Li, K. H. Luo, Y. L. He, Y. J. Gao, and W. Q. Tao. Coupling lattice boltzmann model for simulation of thermal flows on standard lattices. Phys. Rev. E, 85:016710, Jan 2012.

[35] Chih-Hao Liu, Kuen-Hau Lin, Hao-Chueh Mai, and Chao-An Lin. Thermal boundary conditions for thermal lattice boltzmann simulations. Computers & Mathematics with Applications, 59(7):2178–2193, 2010.

[36] Massimo Mannarelli, Cristina Manuel, and Laura Tolos. Phonon contribution to the shear viscosity of a superfluid fermi gas in the unitarity limit. arXiv e-print 1212.5152, December 2012.

[37] P. Massignan, Georg Morten Bruun, and Henrik Smith. Viscous relaxation and collective oscillations in a trapped fermi gas near the unitarity limit. Physical Review A, 71(3):033607, 2005.

[38] K. M. O'Hara, S. L. Hemmer, M. E. Gehm, S. R. Granade, and J. E. Thomas. Observation of a strongly interacting degenerate fermi gas of atoms. Science, 298(5601):2sc179–2182, 2002.

[39] K. M. O'hara, S. L. Hemmer, M. E. Gehm, S. R. Granade, and J. E. Thomas. Observation of a strongly interacting degenerate fermi gas of atoms. Science, 298(5601):2179–2182, 2002.

[40] Y Peng, C Shu, and YT Chew. Simplified thermal lattice boltzmann model for incompressible thermal flows. Physical Review E, 68(2):026701, 2003.

[41] Paul Romatschke. New developments in relativistic viscous hydrodynamics. arXiv e-print 0902.3663, February 2009. Int.J.Mod.Phys.E19:1-53,2010.

[42] Paul Romatschke and Ryan Edward Young. Implications of hydrodynamic fluctuations for the minimum shear viscosity of the dilute fermi gas at unitarity. Phys. Rev. A, 87:053606, May 2013.

[43] Gautam Rupak and Thomas Schfer. Shear viscosity of a superfluid fermi gas in the unitarity limit. Physical Review A, 76(5):053607, 2007.

[44] Thomas Schaefer. In search of the perfect fluid. (0906.5399), June 2009. AIP Conf.Proc.1182:755-758,2009.

[45] Thomas Schaefer. Dissipative fluid dynamics for the dilute fermi gas at unitarity: Free expansion and rotation. Physical Review A, 82(6):063629, 2010.

[46] Thomas Schaefer and Clifford Chafin. Scaling flows and dissipation in the dilute fermi gas at unitarity. In The BCS-BEC Crossover and the Unitary Fermi Gas, pages 375–406. Springer, 2012.

[47] Thomas Schäfer and Derek Teaney. Nearly perfect fluidity: from cold atomic gases to hot quark gluon plasmas. Reports on Progress in Physics, 72(12):126001, 2009.

[48] Thomas Schfer and Derek Teaney. Nearly perfect fluidity: from cold atomic gases to hot quark gluon plasmas. Reports on Progress in Physics, 72(12):126001, 2009.

[49] XIAOWEN SHAN, XUE-FENG YUAN, and HUDONG CHEN. Kinetic theory representation of hydrodynamics: a way beyond the navier–stokes equation. Journal of Fluid Mechanics, 550:413–441, 2 2006.

[50] D. T. Son. Vanishing bulk viscosities and conformal invariance of the unitary fermi gas. Physical review letters, 98(2):020604, 2007.

[51] Sauro Succi. The lattice Boltzmann equation: for fluid dynamics and beyond. Oxford university press, 2001.

[52] Steffen Weinstock. Boltzmann collision term. Physical Review D, 73(2):025005, 2006.

[53] Gabriel Wlaz\lowski, Piotr Magierski, and Joaqun E. Drut. Shear viscosity of a unitary fermi gas. Physical Review Letters, 109(2):020406, 2012.